Cold-atom quantum simulator for string and hadron dynamics in non-Abelian lattice gauge theory

Raka Dasgupta [1,*] and Indrakshi Raychowdhury [2,3,†]

[1]*Department of Physics, University of Calcutta, 92 A. P. C. Road, Kolkata 700009, India*

[2]*Maryland Center for Fundamental Physics and Department of Physics, University of Maryland, College Park, Maryland 20742, USA*

[3]*BITS-Pilani, K. K. Birla Goa Campus, Zuarinagar, Goa 403726, India*

(Received 11 October 2020; accepted 2 February 2022; published 22 February 2022)

We propose an analog quantum simulator for simulating real-time dynamics of $(1+1)$-dimensional non-Abelian gauge theory well within the existing capacity of ultracold-atom experiments. The scheme calls for the realization of a two-state ultracold fermionic system in a one-dimensional bipartite lattice, and the observation of subsequent tunneling dynamics. Being based on the loop string hadron formalism of $SU(2)$ lattice gauge theory, this simulation technique is completely $SU(2)$ invariant and simulates accurate dynamics of physical phenomena such as string breaking and/or pair production. The scheme is scalable and particularly effective in simulating the theory in the weak-coupling regime, and also a bulk limit of the theory in the strong-coupling regime up to certain approximations. This paper also presents a numerical benchmark comparison of the exact spectrum and real-time dynamics of lattice gauge theory to that of the atomic Hamiltonian with an experimentally realizable range of parameters.

DOI: 10.1103/PhysRevA.105.023322

I. INTRODUCTION

Gauge field theories constitute an exceptionally powerful theoretical framework that describes at least three of the four fundamental interactions of nature. Non-Abelian gauge symmetry lies at the heart of the standard model of particle physics. Quantum chromodynamics (QCD), which is an SU(3) gauge theory, can accurately represent quark-gluon interactions. In 1974, Wilson proposed a regularization of the gauge theory on space-time lattices [1] that exhibits quark confinement in the strong-coupling limit. Wilson's lattice gauge theory (LGT) has been used extensively over the past four to five decades because one can perform lattice QCD calculations by Monte Carlo simulations [2]. The world's largest supercomputing resources are now being employed for the same [3].

Although the lattice QCD numerical scheme is very efficient, there is the infamous "sign problem" that limits its applicability [4]. For example, it cannot handle systems with finite and nonzero density or calculate real-time dynamics within the Euclidean framework. Following Feynman's visionary idea [5], quantum simulation of lattice QCD offers hope to address these issues. With the recent technological progresses, there has been a surge of interest towards developing quantum algorithms to study gauge theories using both digital and analog approaches [6–13]. However, the progress in quantum simulation of non-Abelian gauge theories lags far behind its Abelian counterparts. The present paper outlines a scheme for simulating real-time dynamics of a non-Abelian gauge theory in an analog way. In particular, we demonstrate the simulation of a manifestly gauge-invariant framework, namely, a loop-string-hadron (LSH) formalism [14] of $SU(2)$ gauge theory. This scheme successfully bypasses the nontrivial task of imposing the non-Abelian gauge invariance (local constraints) additionally.

The concept of analog quantum simulation involves mimicking a quantum system described by a Hamiltonian (simulated Hamiltonian) by a different quantum system described by some other Hamiltonian (simulating Hamiltonian). Systems of ultracold atoms [15] or ions [16] trapped in optical lattices serve as excellent quantum simulators, as the relevant parameters can be precisely measured and controlled. It can be recalled that though the experimental realization of Bose-Einstein condensates and trapped ultracold fermions [17–23] initially inspired studies on the macroscopic quantum coherent phenomena only [24–26], soon it was discovered that ultracold atoms can serve as wonderful testing grounds for other branches of physics as well. The atom-atom scattering length (and thus, the interaction strength) in ultracold gases can be varied across a wide range via Feshbach resonances. The creation of optical lattices [27] by using two counterpropagating coherent laser beams took this tunability a step further, as the size, shape, and dimensionality of the lattice could be easily controlled. In the past, cold-atom systems have successfully emulated a rich variety of systems and addressed problems in disordered systems, spin liquids, superconductivity, nuclear pairing, artificial gauge fields, and topology [28–30]. Advanced cooling and trapping methods have now led to quantum engineering at an unparalleled precision level. This allows for each individual atom to be monitored, and one can have a perfect quantum simulator.

Over the last few years, there has been a continuous pursuit of using cold-atom systems for analog quantum simulating both Abelian and non-Abelian lattice gauge theories. Mostly

*rdphy@caluniv.ac.in

†indrakshir@goa.bits-pilani.ac.in

based on the Kogut-Susskind (KS) formalism [31–34] as well as quantum link model (QLM) formulation [35–37] and also Abelian Higgs model [38–40], these schemes involved a careful designing of the setup so that the system remains in the gauge-invariant Hilbert space throughout the dynamics. Quantum simulating non-Abelian gauge theories using Rydberg atom gates [41] was also proposed.

Following the first experimental demonstration of a digital quantum simulation of a lattice Schwinger model [42], a density-dependent quantum gauge field was experimentally demonstrated [43], which is useful for simulating dynamics of $\mathbb{Z}_2$ gauge theory. The first analog quantum simulation of $\mathbb{Z}_2$ gauge theory on a two staggered site lattice by cold-atom quantum simulator was reported in [44]. The first experiment demonstrating a scalable quantum simulation of continuous gauge theory [45] has also been reported recently.

The major difficulty in any Hamiltonian simulation of gauge theory is to impose the local constraints (Gauss law) and to keep the dynamics confined within the physical Hilbert space that satisfies the constraint. Recently, such a gauge invariance has been experimentally demonstrated for analog simulation of $U(1)$ gauge theory on a sufficiently large lattice [46]. The notion of gauge invariance becomes manyfold complicated for a non-Abelian theory such as $SU(2)$ where there exists more than one mutually noncommuting constraint at each lattice site. That might be a reason why a practically or immediately realizable analog quantum simulation scheme for simulating dynamics even with the simplest non-Abelian, continuous gauge group such as $SU(2)$ in $(1+1)$ dimensions is absent in the literature to date.

We aim to quantum simulate the same, i.e., $SU(2)$ lattice gauge theory on a $(1+1)$-dimensional lattice described by the KS Hamiltonian [47]. In a recent study [48], it has been demonstrated that amongst many variants of Hamiltonian formulation of non-Abelian gauge theories [49–54], the LSH formalism [14] is the most convenient and computationally least expensive one for $(1+1)$ dimensions within the scope of classical computation. The reason is, being a manifestly gauge invariant formalism, the LSH Hamiltonian describes the dynamics of only relevant physical degrees of freedom. In a one-dimensional (1D) spatial lattice, that is precisely the dynamics of strings and hadrons. It can be shown [48,55] that in $(1+1)$ dimensions any gauge theory with open boundary conditions can be mapped to a theory of only fermions, i.e., equivalent to the XYZ model and hence much simpler to analyze. The LSH formalism shares many features of this purely fermionic formalism but can actually be generalized to periodic boundary conditions as well as to higher dimensions [14].

The present paper exploits this versatility of LSH formalism of $SU(2)$ gauge theory. Here, different parameter regimes of $SU(2)$ gauge theory are mapped to different parameter regimes of an atomic Hamiltonian: that of an ionic Hubbard model. We consider the half-filled Hubbard model to be exactly equivalent to the gauge theory Hilbert space containing a strong-coupling vacuum (no matter or antimatter state). We show that the spectrum, obtained with exact diagonalization of both the simulating and simulated systems, compared remarkably in the weak-coupling regime. We also provide a benchmark comparison of the dynamics of the atomic system directly mapped to the pair production-string breaking dynamics of the low-energy sector of $SU(2)$ gauge theory. The numerical analysis employs parameters and experimental setups already realized with ultracold-atom systems. We demonstrate two key points.

(i) The full gauge theory Hamiltonian can be reduced to an approximated LSH Hamiltonian, which, in turn, can be perfectly mimicked by the atomic system to the low-energy dynamics in the weak-coupling limit of gauge theory.

(ii) For the strong- and intermediate-coupling regimes, the difference between the full gauge theory Hamiltonian and the approximated Hamiltonian is slightly more prominent, but it can be compensated by tuning the on-site interaction parameter of the Hubbard Hamiltonian.

Thus, one can still access the dynamics of strings and hadrons in presence of a background gauge field in the bulk limit of the lattice. Further improvements of this scheme to include dynamical gauge fields in the higher dimensions, and also generalization to $SU(3)$ gauge theory, will take us close to quantum simulating the full QCD.

The plan of the paper is as follows: Sec. II contains the minimal details of the lattice gauge theory Hamiltonian including the LSH framework at different coupling regimes that we aim to quantum simulate. The simulating Hamiltonian is discussed in Sec. III, including the atomic system to be used for the quantum simulation scheme, i.e., a fermionic Hubbard model on a bipartite lattice and specification of the parameters of the simulating Hamiltonian to simulate the gauge theory in a wide range of coupling regimes. In Sec. IV the proposed experimental setup is described. Section V contains numerical study and comparison of the spectrum and real-time dynamics of both the simulating and simulated systems using the parameters for the proposed experimental scheme. Finally, in Sec. VI the results are summarized and future prospects are discussed.

II. THE THEORY TO BE SIMULATED

In this section, we briefly review the theory we would like to simulate (Sec. II A), discuss different parameter regimes of interest (Sec. II B), propose a mean-field ansatz (Sec. II C), and apply the ansatz to a gauge invariant formalism for the same theory (Sec. II D). Finally, the Hamiltonian we quantum simulate is presented (Sec. II E).

A. Kogut-Susskind Hamiltonian

Hamiltonian or canonical formulation of lattice gauge theories was developed by Kogut and Susskind [47] right after Wilson introduced lattice gauge theory originally in Euclidean formalism [1]. In the classical computing era, lattice gauge theory calculations have explored the original Euclidean formulation extensively, but the Hamiltonian framework remained a relatively uncharted territory. However, the interest in the Hamiltonian description of lattice gauge theories is renewed, as it turns out to be the natural framework to work with in the upcoming quantum simulation and computation era. The mostly used formalism in this context is the quantum link model representation of gauge theory as it provides a finite dimensional representation of the gauge fields. There

is a drawback though: in smaller dimensions, that are accessible by present-day quantum technology, the quantum link model does not have the desired spectrum as obtained with the original Kogut-Susskind Hamiltonian [48,49]. In this paper we consider the original Kogut-Susskind Hamiltonian for the simplest non-Abelian gauge group, i.e., $SU(2)$, and proceed to construct a quantum simulator for the same in $(1+1)$ dimensions.

The KS Hamiltonian describing $SU(2)$ Yang-Mills theory coupled to staggered fermions in $(1+1)$ dimensions (1D spatial lattice and continuous time) [47] can be written as

$$H^{(\mathrm{KS})} = H_E^{(\mathrm{KS})} + H_M^{(\mathrm{KS})} + H_I^{(\mathrm{KS})}, \tag{1}$$

where $H_E^{(\mathrm{KS})}$ corresponds to the electric part of the Hamiltonian given by

$$H_E^{(\mathrm{KS})} = \frac{g^2 a}{2} \sum_{j=0}^{N-1} \sum_{a=1}^{3} E^a(j) E^a(j). \tag{2}$$

Here,

$$\sum_{a=1}^{3} E^a(j) E^a(j) = \sum_{a=1}^{3} E_L^a(j) E_L^a(j) = \sum_{a=1}^{3} E_R^a(j) E_R^a(j)$$

for left and right electric fields $\mathbf{E}_{L/R}$ associated with a link connecting sites j and $j+1$.

The staggered fermionic matter ψ in the fundamental representation of $SU(2)$ consisting of two components $\binom{\psi_1}{\psi_2}$ yields a staggered mass term:

$$H_M^{(\mathrm{KS})} = m \sum_{j=0}^{N} (-1)^j [\psi^\dagger(j)\psi(j)]. \tag{3}$$

$H_I^{(\mathrm{KS})}$ denotes interaction between the fermionic and gauge fields and is given by

$$H_I^{(\mathrm{KS})} = \frac{1}{2a} \sum_{j=0}^{N-1} [\psi^\dagger(j) U(j) \psi(j+1) + \mathrm{H.c.}]. \tag{4}$$

The gauge link $U(j)$ is a 2×2 unitary matrix defined on the link connecting sites j and $j+1$. A temporal gauge is chosen to derive the above Hamiltonian which sets the gauge link along the temporal direction equal to unity.

The color electric fields $E_{L/R}^a$ are defined at the left L and right R sides of each link and they satisfy the following commutation relations [$SU(2)$ algebra] at each end:

$$\begin{aligned} \left[E_L^a(j), E_L^b(j')\right] &= i\epsilon^{abc} \delta_{jj'} E_L^c(j), \\ \left[E_R^a(j), E_R^b(j')\right] &= i\epsilon^{abc} \delta_{jj'} E_R^c(j'), \\ \left[E_L^a(j), E_R^b(j')\right] &= 0, \end{aligned} \tag{5}$$

where ϵ^{abc} is the Levi-Civita symbol. The electric fields and the gauge link satisfy the following quantization conditions at each site:

$$\begin{aligned} \left[E_L^a(j), U(j')\right] &= -\frac{\sigma^a}{2} \delta_{jj'} U(j), \\ \left[E_R^a(j), U(j')\right] &= U(j) \delta_{jj'} \frac{\sigma^a}{2}, \end{aligned} \tag{6}$$

where σ^a are the Pauli matrices. The Hamiltonian in (1) is gauge invariant as it commutes with the Gauss law operator

$$G^a(j) = E_L^a(j) + E_R^a(j-1) + \psi^\dagger(j) \frac{\sigma^a}{2} \psi(j) \tag{7}$$

at each site j. The physical sector of the Hilbert space corresponds to the space consisting of states annihilated by (7). Solving the non-Abelian Gauss laws at each site j as given in (7) is nontrivial and engineering the same in an analog experiment is the most difficult job.

In a very recent work [48], all available formalisms for non-Abelian gauge theory with gauge group $SU(2)$ in $(1+1)$ dimensions have been analyzed and compared in terms of their applicability in Hamiltonian simulation. As concluded in [48], the recently developed LSH formalism [14] enjoys two unique advantages: (i) it is exactly equivalent to the original Kogut-Susskind Hamiltonian and (ii) it removes the nontrivial steps (computational costs) required in the original Hamiltonian formulation to contain the dynamics in the gauge invariant sector of LGT Hilbert space. The second advantage becomes particularly important in designing an analog or digital quantum simulator [46,56]. That is why we choose the LSH framework to describe gauge theory and map the same to an atomic Hamiltonian. It is already established [48] that the original Kogut-Susskind Hamiltonian and the LSH Hamiltonian (given in the Appendix A) share identical spectra and hence generate the same dynamics. At this point we must mention that all the feasible and implemented past proposals involve QLM formulation of lattice gauge theory, that in lower dimension exhibits a completely different spectrum as well as a different Hilbert space than that of the Kogut-Susskind Hamiltonian.

B. The two coupling regimes

It is convenient to scale the Hamiltonian $H^{(\mathrm{KS})}$ given in (1) as per [57], so as to make it dimensionless:

$$\begin{aligned} \tilde{H} &= \frac{2}{g^2 a} H^{(\mathrm{KS})} \\ &= \underbrace{\sum_j E^2(j)}_{\tilde{H}_E} + \underbrace{\mu_0 \sum_j (-1)^j [\psi^\dagger(j)\psi(j)]}_{\tilde{H}_M} \\ &\quad \underbrace{+ x_0 \sum_j [\psi^\dagger(j) U(j) \psi(j+1) + \mathrm{H.c.}]}_{\tilde{H}_I}. \end{aligned} \tag{8}$$

Here, $x_0 = \frac{1}{g^2 a^2}$ and $\mu_0 = 2\sqrt{x_0} \frac{m}{g}$ are dimensionless coupling constants of the theory. Evolving this $\tilde{H}$ with scaled time (from zero to $\tilde{\tau}$),

$$\tilde{\tau} = \frac{\tau_{\mathrm{gauge}}}{x_0} \tag{9}$$

is due to the unitary operator:

$$\begin{aligned} \mathcal{U}(\tilde{\tau}) &= \exp\left(-i\tilde{H}\tilde{\tau}\right) \\ &= \exp\left(-i \frac{2}{g^2 a} H^{(\mathrm{KS})} g^2 a^2 \tau_{\mathrm{gauge}}\right) \\ &= \exp\left(-i 2a H^{(\mathrm{KS})} \tau_{\mathrm{gauge}}\right). \end{aligned} \tag{10}$$

Here, $2aH^{(\mathrm{KS})}$ is another scaled Hamiltonian with dimensionless parameters given by

$$2aH^{(\mathrm{KS})} = \frac{1}{x_0}\sum_x E^2(x) + 2\frac{m}{g}\frac{1}{\sqrt{x_0}}\sum_j (-1)^j[\psi^\dagger(j)\psi(j)] + \sum_j [\psi^\dagger(j)U(j)\psi(j+1) + \mathrm{H.c.}]. \quad (11)$$

The strong-coupling limit is defined for $x_0 \to 0$, where the interaction part of the Hamiltonian becomes less dominant as evident from both (8) and (11). On the other hand, in the weak-coupling limit defined at $x_0 \to \infty$, the interaction part of the Hamiltonian becomes the most important term that cannot be treated perturbatively. These scaling rules work equivalently on the LSH Hamiltonian defined in (A18)–(A20) as the LSH Hamiltonian is exactly equivalent to the original Kogut-Susskind Hamiltonian.

In the strong-coupling regime, lattice gauge theory shows the desired physics such as quark confinement and finite mass gap. In this limit, the interaction terms in (4) that involve transitions between different eigenstates of the electric-field operator become insignificant, and hence in the Hamiltonian diagonal terms dominate over the off-diagonal ones in the strong-coupling basis.[1] As $x_0 \to 0$, only very small electric flux configurations on the lattice contribute to the low-energy sector of the theory. In this regime, lattice Hamiltonian matrices can be analyzed perturbatively with the electric part as the unperturbed Hamiltonian. Order by order perturbation corrections yield a finite dimensional Hilbert space, within a cutoff imposed on the bosonic quantum number corresponding to gauge flux. The computation cost rises exponentially with increasing Hilbert-space dimension, that grows with system size as well as cutoff [48]. As a result, calculating Hamiltonian dynamics for an arbitrary large system even with the largest possible computer seems impossible. However, the continuum limit of the LGT lies in the opposite regime, where $x_0 \to \infty$ ($g \to 0, a \to 0$) together with the bulk limit, i.e., lattice size $N \to \infty$. In this regime, the dynamics becomes heavily cutoff sensitive. Here all possible electric flux states contribute to the low-energy spectrum with major contributions coming from strong-coupling basis states with electric flux values to grow larger with $x_0 \to \infty$. The Hamiltonian moves away from diagonal structure as (4) becomes dominant. As a whole, analyzing the weak-coupling limit of lattice gauge theory is extremely difficult on a classical computer except for some extrapolation techniques of strong-coupling analysis.

Now, we propose a mean-field ansatz for the low-energy sector of the gauge theory Hilbert space in the weak-coupling regime. In the next section, we propose an analog quantum simulator to simulate the dynamics of gauge theory in this regime. However, this particular proposal accurately simulates the dynamics of gauge theory beyond this particular regime as well, within the mean-field ansatz. Quantum simulation of the intermediate-coupling regime of the full $SU(2)$ gauge theory involves suitable tuning of atomic interactions as described in the later part of this paper.

[1]For LGT, the natural and most convenient basis is formed out of eigenstates of the electric-field operator. The tensor product of the fermionic occupation number basis and electric-field basis constitutes the full Hilbert space. This particular basis, being the eigenbasis of the diagonal Hamiltonian ($H_E + H_M$) in the $g \to \infty$ limit, is called the strong-coupling basis of LGT.

C. Weak-coupling limit: Mean-field ansatz

As stated earlier, we choose the LSH representation of the Kogut-Susskind Hamiltonian (given in Appendix A) as it provides the most convenient and economic description of the physical degrees of freedom and their dynamics. The LSH basis is characterized by three integer quantum numbers

$$n_l(j) \in (0,\infty)\&n_i(j), n_o(j) \in (0,1) \quad (12)$$

for each site j

The strong-coupling vacuum of the theory is defined by the zero electric flux state. In the LSH formalism, the same state is given by $n_l = 0$ in (12) at all lattice sites. However, as one approaches the weak-coupling regime, the low-energy spectrum of the theory contains states that carry large fluxes. In [58], a weak-coupling vacuum ansatz was proposed and justified for the $(2+1)$-dimensional pure $SU(2)$ gauge theory within the prepotential framework. In that proposal, each lattice site contains a large but mean value for the local loop quantum numbers. The $(1+1)$-dimensional version of that ansatz within the LSH framework (i.e., prepotential + staggered matter) would be equivalent to each site containing more and more gauge fluxes, i.e., $n_l \gg 0$, for all sites as one approaches the weak-coupling limit $g \to 0$. As discussed before, the incoming flux or boundary flux l_i fixes the bosonic loop quantum numbers n_l at each lattice site for any configurations of n_i and n_o throughout the lattice as per (A30). Hence, choosing $l_i \gg 0$ for any finite lattice would result in

$$n_l(j) = l_i \equiv n_l \ \ \forall j. \quad (13)$$

D. Approximate Hamiltonian

In this section, we present a particular form of LSH Hamiltonian that we would like to simulate. This is derived from the Hamiltonian given in (A18)–(A20), that generates the spectrum of the original Kogut-Susskind Hamiltonian discussed before.

1. Electric Hamiltonian

The electric part of the LSH Hamiltonian as given in (A18) can be written as

$$H_E^{(\mathrm{LSH})} = \frac{g^2 a}{2}\sum_j h_E(j). \quad (14)$$

At each site j, depending upon the fermionic quantum numbers n_i and n_o, the local contribution to electric energy is given

by

n_i	n_o	h_E
0	0	$\frac{n_l}{2}\left(\frac{n_l}{2}+1\right)$
0	1	$\frac{n_l+1}{2}\left(\frac{n_l+1}{2}+1\right)$.
1	0	$\frac{n_l}{2}\left(\frac{n_l}{2}+1\right)$
1	1	$\frac{n_l}{2}\left(\frac{n_l}{2}+1\right)$

(15)

The site index (j) is omitted in the above equation as it is on one particular site. Within the average electric-field ansatz, i.e., for $n_l(j) = n_l \Rightarrow h_E(j) = h_E$ for all sites j, we have

$$H_E^{(\text{approx})} = \frac{g^2 a}{2} N h_E^0 \tag{16}$$

where N is the total number of staggered sites on the lattice and $h_E^0 = \frac{n_l}{2}(\frac{n_l}{2}+1)$. Note that, for $n_l \gg 0$, one can actually consider $h_E^0 = h_E \equiv \frac{n_l^2}{4}$.

At any site j, the onsite electric energy $h_E(j)$ differs from h_E^0 if $n_i(j) = 0, n_o(j) = 1$, and that difference, that is relevant in the strong-coupling regime (for $n_l > 0$), is given by

$$\Delta h_E = \frac{n_l+1}{2}\left(\frac{n_l+1}{2}+1\right) - h_E^0 = \frac{n_l}{2} + \frac{3}{4}. \tag{17}$$

This correction term to $H_E^{(\text{approx})}$ is particularly important for the strong- as well as intermediate-coupling regime, where we consider the mean value of the gauge flux, that is not very large compared to that considered in the weak-coupling regime. Within the mean-field ansatz the total electric part of the LSH Hamiltonian is given by

$$H_E^{(\text{LSH})} = \frac{g^2 a}{2}\left[N h_E^0 + \sum_{\{j'\}}\left(\frac{n_l}{2}+\frac{3}{4}\right)\right] \tag{18}$$

where $\{j'\}$ denotes the sites with fermionic configuration $n_i(j') = 0, n_o(j') = 1$. In the bulk limit of the lattice, the occurrence of j' will be $N/4$ for the N site lattice. Hence, the total mean-field electric Hamiltonian in the bulk limit is given by

$$H_E^{(\text{mLSH})} = \frac{g^2 a}{2}\left[N\frac{n_l}{2}\left(\frac{n_l}{2}+1\right) + \frac{N}{4}\left(\frac{n_l}{2}+\frac{3}{4}\right)\right]. \tag{19}$$

2. Mass Hamiltonian

The mass term (A19), being independent of gauge field configuration, remains the same in the mean-field ansatz, and for both the strong- and weak-coupling regime:

$$H_M^{(\text{approx})} = m\sum_j (-1)^j[\hat{n}_i(j) + \hat{n}_o(j)]. \tag{20}$$

3. Interaction Hamiltonian

The matter-gauge field interaction term is the most complicated within the LSH framework as detailed in (A20). In the strong-coupling limit of the theory, this particular term gives small contribution to the Hamiltonian (see Sec. II B) and can be treated perturbatively. However, in the weak-coupling regime, this term becomes significant. The purpose of the present approximation scheme is to bring the interaction Hamiltonian into a simple form, yet describing matter gauge dynamics in the weak-coupling regime.

The approximation scheme that we follow is replacing the local loop quantum numbers $n_l(j)$ by a constant $n_l \gg 0$ at all lattice sites. The interaction Hamiltonian given in (A20) can be written as

$$H_I^{\text{LSH}} = \frac{1}{2a}\sum_{j=0}^{N-2} h_I(j, j+1) \tag{21}$$

where

$$h_I(j, j+1) = h_I^1(j, j+1) + h_I^2(j, j+1) + h_I^3(j, j+1) + h_I^4(j, j+1). \tag{22}$$

Each of these terms can be further decoupled into left (L) and right (R) parts located at site j and site $j+1$, respectively:

$$h_I^{[s]}(j, j+1) = h_I^{[s]}(L) h_I^{[s]}(R)\ , [s] = 1, 2, 3, 4. \tag{23}$$

Now, considering each term separately, one would obtain the following:

$$h_I^{[1]}(L) = \frac{1}{\sqrt{\hat{n}_l + \hat{n}_o(j)[1-\hat{n}_i(j)]+1}}\hat{\chi}_o^+(\lambda^+)^{\hat{n}_i(j)}\sqrt{\hat{n}_l + 2 - \hat{n}_i(j)} = \hat{\chi}_o^+(\lambda^+)^{\hat{n}_i(j)}\hat{C}_1(L), \tag{24}$$

$$h_I^{[2]}(L) = \frac{1}{\sqrt{\hat{n}_l + \hat{n}_o(j)[1-\hat{n}_i(j)]+1}}\hat{\chi}_o^-(\lambda^-)^{\hat{n}_i(j)}\sqrt{\hat{n}_l + 2[1-\hat{n}_i(j)]} = \hat{\chi}_o^-(\lambda^-)^{\hat{n}_i(j)}\hat{C}_2(L), \tag{25}$$

$$h_I^{[3]}(L) = \frac{1}{\sqrt{\hat{n}_l + \hat{n}_o(j)[1-\hat{n}_i(j)]+1}}\hat{\chi}_i^+(\lambda^-)^{1-\hat{n}_o(j)}\sqrt{\hat{n}_l + 2\hat{n}_o(j)} = \hat{\chi}_i^+(\lambda^-)^{1-\hat{n}_o(j)}\hat{C}_3(L), \tag{26}$$

$$h_I^{[4]}(L) = \frac{1}{\sqrt{\hat{n}_l + \hat{n}_o(j)[1-\hat{n}_i(j)]+1}}\hat{\chi}_i^-(\lambda^+)^{1-\hat{n}_o(j)}\sqrt{\hat{n}_l + 1 + \hat{n}_o(j))} = \hat{\chi}_i^-(\lambda^+)^{1-\hat{n}_o(j)}\hat{C}_4(L) \tag{27}$$

and

$$h_I^{[1]}(R) = \hat{\chi}_o^-(\lambda^+)^{1-\hat{n}_i(j+1)}\frac{\sqrt{\hat{n}_l + [1+\hat{n}_i(j+1)]}}{\sqrt{\hat{n}_l + \hat{n}_i(j+1)[1-\hat{n}_o(j+1)]+1}} = \hat{\chi}_o^-(\lambda^+)^{1-\hat{n}_i(j+1)}\hat{C}_1(R), \tag{28}$$

$$h_I^{[2]}(R) = \hat{\chi}_o^+(\lambda^-)^{1-\hat{n}_i(j+1)}\frac{\sqrt{\hat{n}_l+2\hat{n}_i}}{\sqrt{\hat{n}_l+\hat{n}_i(j+1)[1-\hat{n}_o(j+1)]+1}} = \hat{\chi}_o^+(\lambda^-)^{1-\hat{n}_i(j+1)}\hat{C}_2(R), \tag{29}$$

$$h_I^{[3]}(R) = \hat{\chi}_i^-(\lambda^-)^{\hat{n}_o(j+1)}\frac{\sqrt{\hat{n}_l+2[1-\hat{n}_o(j+1)]}}{\sqrt{\hat{n}_l+\hat{n}_i(j+1)[1-\hat{n}_o(j+1)]+1}} = \hat{\chi}_i^-(\lambda^-)^{\hat{n}_o(j+1)}\hat{C}_3(R), \tag{30}$$

$$h_I^{[4]}(R) = \hat{\chi}_i^+(\lambda^+)^{\hat{n}_o(j+1)}\frac{\sqrt{\hat{n}_l+2-\hat{n}_o(j+1)}}{\sqrt{\hat{n}_l+\hat{n}_i(j+1)[1-\hat{n}_o(j+1)]+1}} = \hat{\chi}_i^+(\lambda^+)^{\hat{n}_o(j+1)}\hat{C}_4(R). \tag{31}$$

The only approximation made in the above set of equations is $n_l(j), n_l(j+1) \to n_l$, where n_l is the mean-field value. The explicit operator forms of the coefficients $\hat{C}_{[s]}(L/R)$ are the following:

n_i	n_o	$\hat{C}_1(L)$	$\hat{C}_2(L)$	$\hat{C}_3(L)$	$\hat{C}_4(L)$	$\hat{C}_1(R)$	$\hat{C}_2(R)$	$\hat{C}_3(R)$	$\hat{C}_4(R)$
0	0	1	1	1	$\sqrt{\frac{n_l+1}{n_l+2}}$	1	$\sqrt{\frac{n_l}{n_l+1}}$	$\sqrt{\frac{n_l+2}{n_l+1}}$	$\sqrt{\frac{n_l+2}{n_l+1}}$
0	1	$\sqrt{\frac{n_l+2}{n_l+1}}$	$\sqrt{\frac{n_l+2}{n_l+1}}$	$\sqrt{\frac{n_l+2}{n_l+1}}$	$\sqrt{\frac{n_l+2}{n_l+1}}$	1	$\sqrt{\frac{n_l}{n_l+1}}$	$\sqrt{\frac{n_l}{n_l+1}}$	1
1	0	$\sqrt{\frac{n_l+1}{n_l+2}}$	1	1	$\sqrt{\frac{n_l+1}{n_l+2}}$	1	1	1	$\sqrt{\frac{n_l+1}{n_l+2}}$
1	1	$\sqrt{\frac{n_l+1}{n_l+2}}$	1	1	1	$\sqrt{\frac{n_l+2}{n_l+1}}$	$\sqrt{\frac{n_l+2}{n_l+1}}$	$\sqrt{\frac{n_l}{n_l+1}}$	1

(32)

It is clear from the above set of coefficients that in the limit $n_l \gg 0$ all of the coefficients can be approximated to be equal to identity operators, that is, their leading-order contribution. One can expand the coefficients and add corrections order by order. However, for this paper, we confine ourselves to the leading-order contribution only.

In this regime we also approximate $\lambda^\pm$ as an identity operator as per the approximation, $n_l + 1 \approx n_l$. Hence, the approximated interaction Hamiltonian is given by

$$H_I^{(\text{approx})} = \frac{1}{2a}\sum_j [\chi_o^+(j)\chi_o^-(j+1) + \chi_o^-(j)\chi_o^+(j+1) + \chi_i^+(j)\chi_i^-(j+1) + \chi_i^-(j)\chi_i^+(j+1)]. \tag{33}$$

E. The simulated Hamiltonian

In summary, we obtain the following approximate Hamiltonian that acting on the LSH states on the 1D spatial lattice with the boundary flux $l_i \gg 0$ would result in the exact dynamics of the full gauge theory:[2]

$$H_E^{(\text{approx})} = \frac{g^2 a}{2}\sum_j \left[\frac{\hat{n}_l}{2}\frac{\hat{n}_l}{2}\right], \tag{34}$$

[2]In this limit, the Abelian Gauss law constraint (A1) is automatically satisfied as (A15) and (A16) effectively become equal.

$$H_M^{(\text{approx})} = m\sum_j (-1)^j[\hat{n}_i(j) + \hat{n}_o(j)], \tag{35}$$

$$H_I^{(\text{approx})} = \frac{1}{2a}\sum_j [\hat{\chi}_o^+(j)\hat{\chi}_o^-(j+1) + \hat{\chi}_o^-(j)\hat{\chi}_o^+(j+1) + \hat{\chi}_i^+(j)\hat{\chi}_i^-(j+1) + \hat{\chi}_i^-(j)\hat{\chi}_i^+(j+1)]. \tag{36}$$

We present the details of an atomic quantum simulation scheme to simulate this mean-field Hamiltonian in the next section.

III. THE SIMULATING HAMILTONIAN

In this section, we construct an atomic Hamiltonian that can successfully simulate (34)–(36). We describe the relevant quantum system (Sec. III A), and its connection with the LSH Hamiltonian is established (Sec. III B). That the model is well suited for both the weak-coupling and strong-coupling limits of gauge theory is demonstrated in Sec. III C.

A. Atomic Hamiltonian: The Hubbard model on a bipartite lattice

We consider a Fermi-Hubbard model in a one-dimensional lattice. The optical potential is of the form

$$V(x) = -V_L\cos^2(kx). \tag{37}$$

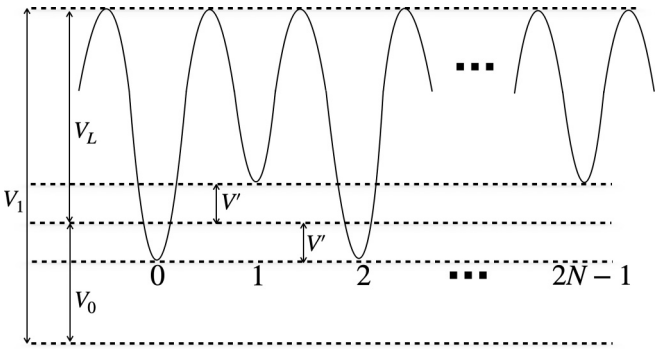

FIG. 1. Structure of the two-color lattice.

The minimum of each well corresponds to the physical lattice site with site index j. $V(x)$ can also act as the trapping potential. Here $V_L > 0$ and $k = \pi/d$, d being the lattice periodicity. Next, energy offsets of V' and $-V'$ are added to the odd and even sites, respectively. So, a bipartite lattice is created, and effectively the lattice spacing is $2d$ now. The structure of this two-color lattice is shown in Fig. 1.

The fermionic atoms can belong to either of its two accessible hyperfine states: we denote them by the symbols $|\uparrow\rangle$ and $|\downarrow\rangle$, respectively. Let $c_\uparrow(j)$ be the fermionic annihilation operator for spin index $\uparrow$ and let $c_\downarrow(j)$ be the fermionic annihilation operator for spin index $\downarrow$, both for site j. The corresponding number operators are $\mathcal{N}_{j\uparrow}$ and $\mathcal{N}_{j\downarrow}$. The total number of fermions at site j is given by $\mathcal{N}(j) = \mathcal{N}_\uparrow(j) + \mathcal{N}_\downarrow(j)$.

The lattice depth V_L can be written as $(V_1 - V_0)$. It is to be noted that V_1 and V_0 are theoretical parameters only, and will be used to make a connection between the atomic Hamiltonian and the LSH Hamiltonian. From an experimental perspective, it is only V_L that is of importance.

The Hamiltonian can be written as

$$H = H_{\text{hopping}} + H_{\text{int}} + H_{V_0} + H_{V'} \tag{38}$$

where, in terms of the tight-binding parameters,

$$H_{\text{hopping}} = -\sum_j t_j[c_\uparrow^\dagger(j)c_\uparrow(j+1) + c_\downarrow^\dagger(j)c_\downarrow(j+1)] + \text{H.c.}, \tag{39}$$

$$H_{\text{int}} = u\sum_j \mathcal{N}_\uparrow(j)\mathcal{N}_\downarrow(j), \tag{40}$$

$$H_{V_0} = \sum_j V_0\mathcal{N}(j), \tag{41}$$

and

$$H_{V'} = V'\sum_{j=\text{odd}} \mathcal{N}(j) - V'\sum_{j=\text{even}} \mathcal{N}(j). \tag{42}$$

Here we have dropped a term $H_{V_1} = \sum_j V_1\mathcal{N}(j)$ from the Hamiltonian, as this provides just a constant energy shift. The details are given in Appendix B.

If the hopping $-t$ is a constant throughout the lattice, this model essentially is a 1D Hubbard model with alternating potential, often termed as the "ionic Hubbard model," defined on a bipartite lattice. Here, in addition to a site-independent hopping $-t$ and the on-site interaction u, there is a difference in the energy offset $2V'$ between sublattice A and sublattice B. This model was originally proposed to study transitions in organic crystals [59], and later found application in the studies of ferroelectric transitions [60]. In the recent past, this model has been experimentally realized [61] in a system of ultracold atoms. So we consider this to be a very suitable candidate to simulate lattice gauge theories.

At half filling, the ionic Hubbard model is capable of describing a band insulator [62]. However, this model has a rich phase diagram, and at higher interatomic interaction strengths can support transitions to different states, including Mott insulator [62], correlated insulator [63,64], antiferromagnetic insulator, and half-metal [64] phases; certain combinations of u and V' can even lead to superfluidity [65]. As we will see in the later part of this paper, we have to carefully choose our parameters such that the entire dynamics remains confined to a single paramagnetic phase in order to mimic the dynamics of gauge theory.

B. Mapping the parameters

We are now in a position to compare the weak-coupling LSH Hamiltonian and the atomic Hamiltonian. For a particular site j, we make the following identification:

$$n_i(j) = \mathcal{N}_\uparrow(j), \qquad n_o(j) = \mathcal{N}_\downarrow(j), \tag{43}$$

$$\chi_i^+(j) = c_\uparrow^\dagger(j), \qquad \chi_i^-(j) = c_\uparrow(j), \tag{44}$$

$$\chi_o^+(j) = c_\downarrow^\dagger(j), \qquad \chi_o^-(j) = c_\downarrow(j), \tag{45}$$

$$m = V'. \tag{46}$$

Also, the magnitude of V_0 has to be chosen to be mapped to the electric part of the gauge theory Hamiltonian for a particular n_l, fixed by the open boundary condition.

The electric term of the approximated LSH Hamiltonian is mapped to

$$H_E^{(\text{approx})} \to \sum_j V_0\mathcal{N}(j). \tag{47}$$

Similarly, the potential V' is fixed by the mapping

$$H_M^{(\text{approx})} \to V'\sum_{j=\text{odd}} \mathcal{N}(j) - V'\sum_{j=\text{even}} \mathcal{N}(j) \tag{48}$$

and the hopping terms are identically related as

$$H_I^{(\text{approx})} \to -t\sum_j [c_\uparrow^\dagger(j)c_\uparrow(j+1) + c_\downarrow^\dagger(j)c_\downarrow(j+1)] + \text{H.c.} \tag{49}$$

Note that there is no term in the weak-coupling LSH Hamiltonian that corresponds to the on-site interaction term (B6). So, in the limit $u \to 0$, one would have a complete mapping between the atomic system and weak-coupling limit of the gauge theory.

We would like to point out that although the LSH Hamiltonian contains explicit bosonic modes $n_l(j)$, these are actually nondynamical in the weak-coupling approximation as discussed before, and hence we do not keep actual bosons in

the atomic system. Instead, we incorporate the effect of these bosons in the potential itself, in the form of a constant energy shift. This enables us to (i) keep n_l uniform for each site and (ii) ensure that the bosonic and the fermionic modes are completely decoupled, as there remains no chance of any boson-fermion scattering.

C. Simulating both weak- and strong-coupling regimes of gauge theory

We now present the features of this proposed scheme that enable one to simulate accurate dynamics of the gauge theory beyond the weak-coupling limit emphasized so far.

It is important to note that this particular scheme assumes mean-field contribution from the loop degrees of freedom, while the two fermionic degrees of freedom describe the dynamics of the theory. The configurations with large incoming flux l_i correspond to low-energy states in the weak-coupling regime. On the other hand, the strong-coupling vacuum is defined to be the state with zero electric flux. This particular scheme calls for choosing a nonzero value of the incoming flux $l_i \geqslant N$ for a N-site staggered lattice, such that all of the fermionic configurations correspond to physical LSH configurations [48]. Physically this amounts to a constant shift in the vacuum energy level as compared to the strong-coupling vacuum of the theory. We propose that different sectors of the gauge theory can be simulated by choosing appropriate values of l_i ($l_i \gg 0$ for weak-coupling theory, $l_i \approx N$ for strong-coupling theory).

Moving away from the weak-coupling approximation, the electric part of the Hamiltonian becomes dominant. This part (2) measures the electric flux contribution of each individual link. Within the LSH framework, it has some contribution from the local loop quantum number n_l as well as from the local string quantum numbers n_i and n_o at the site from where the link starts as given in (A18). One can also express the total electric contribution as a function of local n_l depending on the local fermionic configurations as listed in (15). Thus, the complete on-site contribution to the electric part of the Hamiltonian can be divided into two categories.

(a) For three of the four allowed fermionic configurations at any site (15), the approximated contribution is a function of n_l only [see Eq. (16)].

(b) For the other fermionic configuration, the electric contribution to the Hamiltonian has an additional correction term (17). In our scheme, this correction term (17) is added to (16) for $N/4$ sites (as the probability of obtaining one such particular arrangement of fermions is $1/4$). Therefore, the total correction in the electric Hamiltonian is

$$\Delta H_E^{(\mathrm{LSH})} = \frac{g^2 a}{2}\frac{N}{4}\left(\frac{n_l}{2}+\frac{3}{4}\right). \tag{50}$$

The on-site interaction in the atomic Hamiltonian, which does not have an equivalent in the approximate LSH Hamiltonian, can be tuned to recover the exact contribution of (50). For a Hubbard model at half filling, all the four accessible states $|0\rangle, |\uparrow\rangle, |\downarrow\rangle$, and $|\uparrow\downarrow\rangle$ are equally likely as long as the system remains in the paramagnetic phase. So,

$$N_{|\downarrow\rangle} \approx \frac{N}{4}, N_{|\uparrow\downarrow\rangle} \approx \frac{N}{4}. \tag{51}$$

Here $N_{|\downarrow\rangle}$ denotes the number of sites belonging to state $|\downarrow\rangle$, and $N_{|\uparrow\downarrow\rangle}$ is the number of sites with doublons. N is the total number of lattice sites. It is the doublon configurations that contribute to (B6). Hence, one can utilize the on-site interaction term to recover the exact correction term

$$u\sum_j \mathcal{N}_\uparrow(j)\mathcal{N}_\downarrow(j) = u\frac{N}{4} \Rightarrow u \equiv \frac{g^2 a}{2}\left(\frac{n_l}{2}+\frac{3}{4}\right) \tag{52}$$

in order to match it with (50).

Hence, for the bulk limit of the lattice ($N \gg 0$), we have the maximum overlap of the (mean-field approximated) strong-coupling lattice gauge theory to the Fermi-Hubbard Hamiltonian as

$$H_E^{(\mathrm{mLSH})} \longrightarrow H_{V_0} + H_{\mathrm{int}}, \tag{53}$$

$$H_M^{(\mathrm{LSH})} \longrightarrow H_{V'}, \tag{54}$$

$$H_I^{(\mathrm{approx})} \longrightarrow H_{\mathrm{hopping}} \tag{55}$$

provided we fix V_0 and u such that the system, staying in the desired phase, mimics the dynamics of gauge theory as shown in Fig. 2.

The correction to the approximate interaction Hamiltonian is negligible in the weak-coupling regime, and also insignificant in the strong-coupling limit. In this paper, we do not consider any correction to the interaction term.

We now explicitly calculate the parameters of the atomic Hamiltonian, that has to be tuned in the experiment to simulate desired gauge theory dynamics in different coupling regimes.

1. *Weak-coupling regime of gauge theory: u/t 0*

In this particular regime we consider the scaled Hamiltonian given in (8). Within the approximation scheme done for the equivalent LSH Hamiltonian for a finite lattice given in (34), we consider the bosonic loop quantum number to take the average value:

$$n_l \approx O(10^p) \Rightarrow \tilde{H}_E^{(\mathrm{approx})} \approx O(10^{2p}). \tag{56}$$

For a comparative mass an interaction contribution of the Hamiltonian, i.e.,

$$\tilde{H}_M^{\mathrm{LSH}} \approx O(10^{2p}), \tag{57}$$

$$\tilde{H}_I^{(\mathrm{approx})} \approx O(10^{2(p+p')}), \tag{58}$$

is obtained for the following scaling of parameters:

$$\frac{m}{g} \approx O(10^{p-p'})\,\sqrt{x_0} \approx O(10^{p+p'})\,, \forall p' \in \mathbb{Z}_+. \tag{59}$$

The exact values of the dimensionless parameters of gauge theory can be taken as

$$n_l = \tilde{n}_l \times 10^p, \tag{60}$$

$$\mu_0 = \tilde{\mu}_0 \times 10^{2p}, \tag{61}$$

$$x_0 = \tilde{x}_0 \times 10^{2(p+p')},\ \forall \text{ integer } p, p' \tag{62}$$

$$= 10^{2p} \text{ for the choice, } p' = 0, \tilde{x}_0 = 1. \tag{63}$$

Now, the dynamics of this scaled Hamiltonian $\tilde{H}$ in (8) is to be simulated by the simulating Fermi-Hubbard Hamiltonian

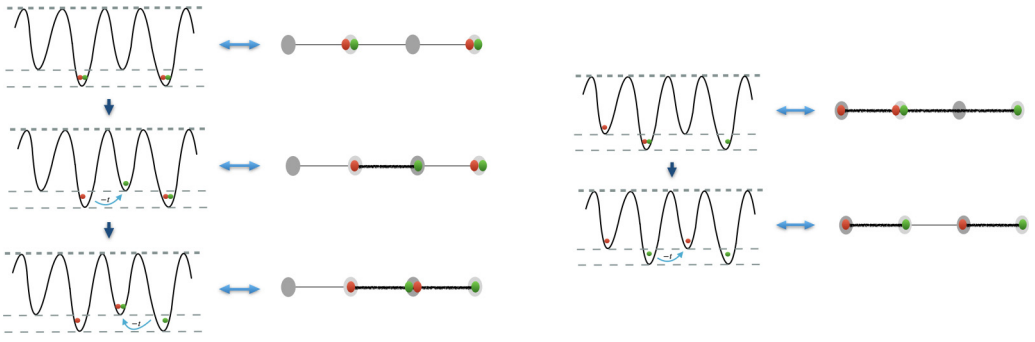

FIG. 2. Dynamics of the 1D ionic Hubbard model mimicking that of $SU(2)$ lattice gauge theory in one spatial dimension. (a) Initial state: fully filled odd sites and empty even sites mimicking the strong-coupling vacuum consisting of no particles ($n_i = 0, n_o = 0$ on even sites) and no antiparticles ($n_i = 1, n_o = 1$ on odd sites). Under Hamiltonian evolution, one atom hops from an odd site to a neighboring even site in the Hubbard model, that mimics creation of a particle antiparticle pair at two neighboring staggered sites of the gauge theory, connected by one unit of flux to form a gauge singlet string configuration. One further hopping as shown in the figure mimics the dynamics in gauge theory as elongation of the string and creation of a baryon on one site. In these three states, the total numbers of particles (antiparticles) for the gauge theory are, respectively, 0, 1, and 2. (b) Ionic Hubbard model dynamics mimicking string breaking dynamics of gauge theory. Starting from a string of length 3 units, pair production occurs and the initial string breaks into two smaller strings.

given in (38) in the time scale $\tilde{\tau}$ as defined in (9), such that

$$\exp(-i\tilde{H}\tilde{\tau}) \longrightarrow \exp(-iH\tau) \tag{64}$$

where H is the atomic Hamiltonian given in (38) with the parameters

$$V' = \tilde{\mu}_0, \tag{65}$$

$$V_0 = \frac{1}{4}\left(\tilde{n}_l^2 + 2\tilde{n}_l\right), \tag{66}$$

$$u = 0, \tag{67}$$

$$t = -1. \tag{68}$$

Here, all the parameters are fixed in units of t. The only choice that we have made in setting the parameters is $p' = 0$ in (62). Gauge theory with a nonzero p' can be equivalently simulated by the same atomic system with tuning V' to smaller values $\tilde{\mu}_0 \times 10^{-2p'}$ in an experiment. This will access all mass values of gauge theory in the quantum simulation protocol.

2. *Strong-coupling regime of gauge theory:* $|u/t| > 1$

We consider the scaled Hamiltonian in (11) in the strong-coupling regime $x_0 < 1$. As discussed earlier, the bulk limit of the Fermi-Hubbard Hamiltonian in the paramagnetic phase will correspond to the exact mean-field electric term (19) and mass term (A19). Although the interaction term is approximated, it will not make a major difference in spectrum and/or dynamics as $x_0 \to 0$ as it is less dominant compared to diagonal terms. Likewise, in the weak-coupling regime, we fix the boundary condition l_i to be a fixed integer, but of $O(1)$. We map the gauge theory Hamiltonian to the Fermi-Hubbard Hamiltonian with parameters

$$V' = 2\frac{1}{\sqrt{x_0}}\frac{m}{g}, \tag{69}$$

$$V_0 = \frac{1}{x_0}\frac{l_i}{4}(l_i + 2), \tag{70}$$

$$u = \frac{1}{x_0}\frac{1}{4}(2l_i + 3), \tag{71}$$

$$t = -1. \tag{72}$$

Here also, all the parameters are fixed in units of t. It is clear from the above relations that for a fixed value of l_i, smaller values of x_0 require larger V_0/t and u/t for the atomic system. However, we will have to be careful to remain in the same paramagnetic phase such that our analysis of compensating errors in the electric Hamiltonian from the uniform potential are well compensated by the self-interaction term. For this purpose, i.e., in order to keep u/t below the critical point for paramagnetic-ferromagnetic phase transition, one cannot really expect to simulate $x_0 \to 0$ under the present scheme. However, one can simulate $x_0 < 1$ as well as $x_0 = 1$ besides accurately simulating intermediate-coupling range $x_0 \approx$ 10–100 as will be demonstrated in the numerical analysis.

Likewise in the weak-coupling case, the simulating and simulated dynamics are comparable up to a factor

$$\tau_{\text{atomic}} = 2a \times \tau_{\text{gauge}}, \tag{73}$$

where a is small but finite in the strong-coupling limit.

In the next section, we propose the precise experimental setup that is close to already performed experiments for the ionic Hubbard model following the above-mentioned scheme, where the strong-coupling regime of lattice gauge theory dynamics is mapped to the ionic Hubbard model with $u/t > 1$, whereas the weak-coupling regime is mapped to the same with $u/t \approx 0$.

IV. EXPERIMENTAL REALIZATION

The experimental scheme calls for the realization of the 1D Fermi-Hubbard model in a bipartite lattice. In the recent past, the ionic Fermi-Hubbard model was experimentally realized in a honeycomb lattice [61], and its bosonic counterpart was implemented on a bipartite checkerboard lattice [66]. Also, a

1D Fermi-Hubbard model was implemented in an experiment by Scherg *et al.* [67]. Both [61] and [67] used a degenerate gas of fermionic ^{40}K of numbers $\approx 10^5$ and 10^4, respectively. We propose that a combination of these two methods can successfully yield a 1D Hubbard model with alternating lattice potentials. The setup, which is very much realizable with current experimental techniques, is described in Sec. IV A. The procedures for preparing the initial states and observing the final dynamics are outlined in Secs. IV B and IV C, respectively. We discuss the possible sources of errors (that can affect the accuracy of the results in this experiment) in Sec. IV D.

A. Proposed setup

The interference pattern of two counterpropagating lasers is used to create an optical lattice. The lattice depth is proportional to the intensity of the laser beam and is measured in units of the recoil energy E_R.

In the experiment by Messer *et al.* [61], first a regular honeycomb lattice was created, and that fixed the hopping parameter t on each bond. Next a staggered energy offset of Δ was independently applied between sites of A and B sublattices. In our 1D structure, an equivalent would be to set up the primary lattice with lattice depth V_L. This fixes the hopping parameter t. Then, on top of it, energy offsets V' and $-V'$ can be independently applied on the odd sites and even sites, respectively, so that the lattice depth is $(V_0 + V')$ for odd sites, and $(V_0 - V')$ for even sites.

Just like the hopping t, the on-site interaction u depends on the lattice depth. However, u can be independently controlled as well, by means of Feshbach resonance. As for the two fermionic states, any two hyperfine states of a particular atom can be employed. In [67], the hyperfine states

$$|\uparrow\rangle = |F = -9/2; m_{\rm F} = -9/2\rangle,$$
$$|\downarrow\rangle = |F = -9/2; m_{\rm F} = -7/2\rangle$$

of ultracold ^{40}K atoms were used. In [61], in addition to the above, the combination

$$|\uparrow\rangle = |F = -9/2; m_{\rm F} = -9/2\rangle,$$
$$|\downarrow\rangle = |F = -9/2; m_{\rm F} = -5/2\rangle$$

was also employed in order to obtain the desired range of u.

In [61], the ionic Hubbard model was studied on a honeycomb lattice. In contrast, our model requires the implementation of the ionic Hubbard model in a simple one-dimensional geometry. Regarding the dimensionality of the system, it may be recalled that in the recent past, ultracold-atom experiments have successfully confined bosonic and fermionic atoms to one dimension. The basic idea is to tightly confine the particles in two transverse directions, and make them weakly confined in the axial direction. Thus, their motions in the transverse directions are completely frozen. So, effectively, these are quasi-1D systems.

For example, in our proposed setup, suppose both V_y and V_z, the potentials in the transverse directions, are kept fixed at a large value (like, $33E_R$ as in [68], or $42E_R$ as in [69]). $V(x)$, the lattice depth in the axial direction, is kept in a range of $5E_R$–$12E_R$. We note that in Hubbard model experiments, the potentials are to be deep enough ($V \geqslant 5E_R$) so that the single-band description of the Hubbard model remains valid. On the other hand, $V(x)$ cannot be as deep as the potentials in the transverse direction, so as to restrict the dynamics in one dimension only. The hopping parameter t is a function of the lattice depth, and can be estimated using the Wannier functions [70].

In Sec. III A, the lattice depth V_L was written as $(V_1 - V_0)$, so different combinations of V_1 and V_0 can result in the same lattice depth. This offers a tremendous advantage in the experimental pursuit, as the same optical lattice can be assumed to be split in different pairs of V_1 and V_0, allowing one to explore a wide range of V_0 values [that, in turn, enables one to access a wide range of x_0 and/or l_i as per (70)]. It is to be noted that both V_1 and V_0 are theoretical parameters in the model that leads to constant shifts in the energy only, bearing no effect on the dynamics of the fermions.

Accordingly, we consider two configurations:
(i) $V_1 = 6E_R$ and $V_0 = 0.5E_R$ and
(ii) $V_1 = 6.5E_R$ and $V_0 = 1E_R$.

In both the cases, the resultant uniform lattice depth V_L is $5.5E_R$ for all the sites. This results in a hopping $t = 0.057E_R$. The combinations we have mentioned translate to

$$\text{(i) } V_0 \approx 8.75t \quad \text{and} \quad \text{(ii)} V_0 \approx 17.5t,$$

respectively. In addition, an offset of V' and $-V'$ is independently applied on the odd and even sites. In our scheme, we choose $V' = 1.6t$ and stick to this value in all our numerical simulations. The on-site interaction u can be controlled by applying a Feshbach field.

To simulate the weak-coupling limit, we restrict ourselves to the weakly interacting atomic limit, $u/t << 1$, and choose $u = 0.1t$. On the other hand, simulation of the strong-coupling limit calls for the realization of the strongly interacting atomic limit, $u/t \gg 1$, and we choose $u \approx 5.5t$. We note that these V'/t and u/t values comfortably fall in the parameter regimes accessed in recent experiments [61,67,71].

B. Initial-state preparation

The initial state has to be prepared in a charge-density-wave (CDW) configuration where all the odd sites are occupied by the fermionic particles and the even sites are completely empty. This can be done using some sort of filtering sequence in the experiment. For example, in [71,72], this was achieved by superposing the primary lattice (with wavelength λ) with an additional long lattice (with wavelength 2λ) in the following way:

$$V(x) = -V_L \cos^2(kx) - \tilde{V}[\cos^2(kx/2 + \phi)] \qquad (74)$$

with $k = 2\pi/\lambda$.

The lattice depths V_L and $\tilde{V}$ and the relative phase ϕ can be adjusted independently. Here V_L stands for the depth of the original (and short) lattice, and $\tilde{V}$ is the depth of the additional long lattice. This long lattice is utilized during the preparation of the initial CDW state. Initially, the long lattice is made quite deep (like $20E_R$, as in [71]), and the short lattice is ramped up to that depth at a nonzero relative phase ϕ to create a tilted lattice of double wells. Now it is so arranged that the odd sites host lower-energy wells than the even sites, and it is possible

to load all atoms in the odd sites only. The tilt offsets are made sufficiently large so that the particles cannot escape from the odd sites and tunnel to the even sites. After loading all the atoms, the longer lattice is switched off, and the short lattice is ramped down to its desired final value (in our case, $5.5E_R$). The offset V' and $-V'$ is added to the odd sites and even sites, respectively, to create the bipartite structure. Now tunneling is possible between adjacent sites, and the dynamics begins.

Moreover, (52) is only valid if $N_{|\downarrow\rangle}$=$N_{|\uparrow\downarrow\rangle} = N/4$ as in (51). Since here the system is initially prepared in a CDW state containing doublons only, this will not hold true in a short initial time span, and the interatomic interaction u will overcompensate the correction term in the electric Hamiltonian. Thus, the dynamics from the atomic Hamiltonian will have a departure from that of the full gauge theory. However, with time, more and more atoms would hop to the adjacent sites and the distribution would get more even across the sites, resulting in $N_{|\downarrow\rangle} \approx N_{|\uparrow\downarrow\rangle}$. So, soon enough, the quantum simulation becomes more accurate, as demonstrated in the numerical results in Sec. V.

C. Observing the dynamics

The observable can be defined as the population imbalance P between the even sites and odd sites, defined as

$$P = \frac{N_e - N_o}{N_e + N_o}. \tag{75}$$

Here N_e is the total number of atoms in the even sites, and N_o is the total number of atoms in the odd sites.

The time evolution of the parameter P is to be studied in order to visualize the particle number dynamics of gauge theory. A site-resolved technique is thus needed to determine the number of atoms on even and odd lattice sites separately. In [71,72], a band-mapping scheme was successfully employed using the long lattice. Once the desired time evolution in the primary (short) lattice is over, the long lattice is introduced again to create the tilted lattice, and tunneling stops. The phase ϕ is chosen in such a way that the odd sites constitute the lower wells in the array of double wells. Now the population distribution across the odd and even sites gets sealed. Next, the depth of the long lattice is ramped to a much higher value, and the atoms in the even sites get transferred to the third Bloch band of the superlattice. Atoms in the odd sites remain in the first band. The density profile in the different bands can be obtained using time-of-flight images and absorption imaging [71].

D. Possible source of experimental errors

The particle-antiparticle pair creation and string breaking in gauge theory are mimicked by the ionic Hubbard model dynamics, and the relevant observable at any instant is P, the averaged population imbalance between even sites and odd sites. Thus, individual site-resolved occupancy data are not required. If the lattice is sufficiently long and if the averaging is done properly (like, in [67], each data point was averaged over four measurements), it is possible to obtain a very accurate value of P. The lattice potential and the sublattice offset, too, can be precisely monitored [61,66].

The only major source of possible experimental errors can be the imperfection in the initial-state preparation. A CDW state can certainly be realized where only the odd sites are occupied, but then those sites can host zero, single, or double occupancy as in [71]. To ensure that all the odd sites have doublons, one needs to monitor the number of atoms precisely. As reported in [61], there is always a systematic uncertainty of 10% in the preparation. However, as demonstrated in the next section, the dynamics is very little affected even with this error margin.

V. SIMULATED DYNAMICS AND OBSERVABLES

In this section, we present numerical analysis of our proposal. The comparison between the spectrum of the simulating and simulated systems is presented in Sec. V A, and the corresponding dynamics is presented in Sec. V B. In Sec. V C, we demonstrate that even if there is an initial error in preparing the system in a perfect CDW state, the dynamics is not affected much, and the departure from the expected result remains well within an acceptable window of tolerance.

A. Spectrum comparison

1. In the weak-coupling regime

We aim to quantum simulate the gauge theory Hamiltonian, with the values of dimensionless parameters given by

$$x_0 = 10^{-10},\ m/g = 1.6 \times 10^{-10}$$

acting on the LSH Hilbert space characterized by

$$n_l = 5 \times 10^5$$

at all sites and corresponding to $p = 5, p' = 0$ in (60)–(62). The fermionic (string) configurations remain completely dynamical as n_i and n_o can take all possible values at sites $0, 1, 2, \ldots, 2N$. Following (65)–(67) we obtain the parameters of the atomic Hamiltonian to be fixed at

$$V_0 = 8.75t, V' = 1.6t, u = 0.1t. \tag{76}$$

Note that we have chosen a feasible but small value of the parameter u. Smaller and smaller values of u will enable us to mimic the dynamics of gauge theory more accurately as we take $p \gg 1$. We perform exact diagonalization for both the Hamiltonians with a small number of sites, that is doable on a PC. Our scheme being completely scalable, the agreement in spectrum as in Fig. 3 holds true for any size of lattice as per experimental capabilities.

2. In the strong-coupling regime

We aim to quantum simulate gauge theory Hamiltonian (11), with the values of dimensionless parameters given by

$$x_0 = 0.69,\ m/g = 1.6.$$

This Hamiltonian acts on LSH Hilbert space characterized by $l_i = 6$ as in (13), while n_i and n_o can take all possible values at sites $0, 1, 2, \ldots, 2N$. Following (69)–(71), the mimicking atomic system is defined by parameters

$$V_0 = 17.5t, V' = 1.6t, u = 5.47t. \tag{77}$$

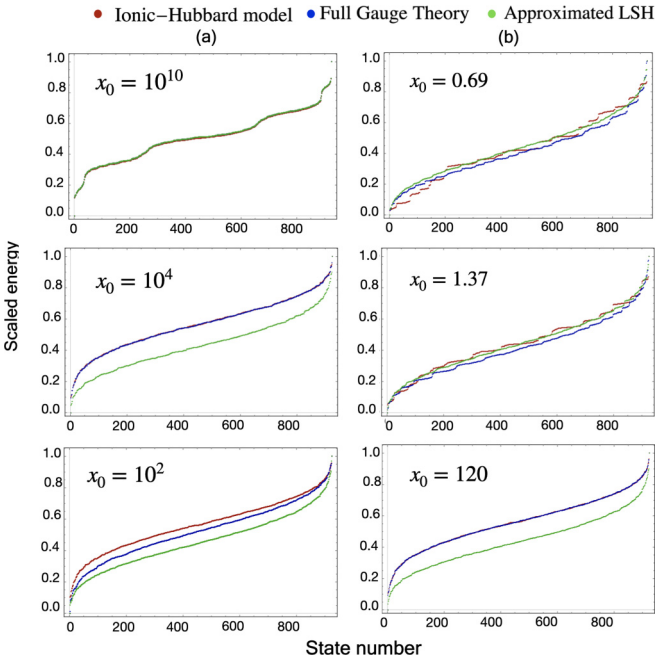

FIG. 3. Spectrum of the ionic Hubbard model, full $SU(2)$ gauge theory (KS or LSH) Hamiltonian (without any approximation), and weak-coupling approximated LSH calculated by exact diagonalization for a six site system and scaled to fit between 0 and 1. (a) The spectrum in the weak-coupling regime of gauge theory with parameters as per (76) for different values of p as discussed in Sec. III C 1. (b) The spectrum obtained for the strong-coupling analysis, for $V_0 = 17.5, 8.75,$ and 0.1, respectively. The spectrum demonstrates that the intermediate-coupling regime is better accessible by strong-coupling analysis if smaller values of V_0 become experimentally feasible. We propose to quantum simulate the strong-coupling spectrum within a mean-field approximation and at the bulk limit, whereas the plots are only for small lattices and hence show magnified deviation of the mean-field spectrum from that of the full gauge theory. The approximated LSH is only valid in the weak-coupling regime and matches with full gauge theory for $p \gg 1$.

Like the weak-coupling case, we also perform exact diagonalization for this case to compare and obtain the spectrum as in Fig. 3. Note that from our analysis we only expect an exact match of spectra in the $N \to \infty$ limit, and that is beyond the scope of exact diagonalization. However, in Fig. 4, we demonstrate that if the lattice size keeps increasing, the agreement between the simulating spectrum and the original spectrum gradually improves. Thus, it is expected that in the bulk limit there would be a perfect agreement. Performing numerical calculations for a longer lattice is beyond the scope of exact diagonalization, and thus the present paper. In principle, it can be carried out using state-of-the-art tensor network techniques, and establish a proper benchmark for the scheme in the strong-coupling regime. However, the tensor network can only calculate a particular (low-energy) sector of the theory with the desired accuracy, and quantum simulation is expected to outperform the same.

However, even with limited computational resources, we make the following observations.

(1) It appears from (69)–(71) that, by increasing V_0/t in the atomic system, one would be able to access smaller and smaller values of the gauge theory parameter x_0. However, the consequence is that, in order to mimic exact strong-coupling dynamics, u/t has to be increased as well.

(2) With an increasing u/t (even for a fixed value of V_0/t), gaps are introduced in the atomic spectrum as the the atomic system experiences a quantum phase transition (see Fig. 5) and enters the Mott insulator phase [73]. Then the system can no longer mimic dynamics of gauge theory as there is no such quantum phase transition in the gauge theory spectrum. Hence, this quantum simulation scheme is not suitable for $x_0 \to 0$.

(3) Instead, if one can arrange the experimental setup to fix V_0/t at a smaller value, the atomic system simulates the intermediate-coupling regime of the full gauge theory reliably. We illustrate such an agreement for $V_0/t = 0.1$ ($x_0 = 120$) in Fig. 3.

B. Simulated dynamics

One important dynamical phenomenon to observe in real-time dynamics in gauge theory is the dynamics of pair production and string breaking as illustrated in Fig. 2. We consider preparing the system in a state in which all even sites are completely empty (no particle) and all odd sites are completely filled (no antiparticle). The real-time Hamiltonian evolution of the atomic system involves atoms hopping from one site to another, simulating the event of pair creation and particle number dynamics of gauge theory. Within the LSH framework, for the no particle–no antiparticle state $|\Psi_0\rangle$ on a 1D lattice of N staggered sites, we define the following quantity to describe particle density:

$$\rho(\tau) = 1 + \frac{1}{N}\langle\Psi_0|\hat{\mathcal{U}}^\dagger(\tau)\hat{\mathcal{O}}\hat{\mathcal{U}}(\tau)|\Psi_0\rangle \tag{78}$$

where $\hat{\mathcal{O}} = \sum_j\{(-1)^j[\hat{n}_i(j) + \hat{n}_o(j)]\}$ and $\mathcal{U}(\tau_{\text{gauge}})$ is defined in (10).

The simulated dynamics in the Hubbard model is measured by the observable P, as defined in (75). Its connection with the particle number dynamics of gauge theory can be obtained by looking at the parameter $1 + P$. In Fig. 6 we plot the quantities against a scaled time $\tau = \tau_{\text{atomic}} = 2a\tau_{\text{gauge}}$ following (9).

As done in the spectrum analysis, we consider the same parameter values for calculating pair-production and string breaking dynamics as well. From the simulated dynamics we can conclude the following.

(1) The proposed simulation scheme simulates the dynamics of weak-coupling gauge theory perfectly and that is evident even from the numerical analysis using a small system. Here the particle density dynamics resulting from (i) full gauge theory, (ii) the approximated LSH theory, and (iii) the atomic Hamiltonian all agree very well.

(2) The difference between the actual dynamics due to the original Hamiltonian and the dynamics due to the approximated Hamiltonian is quite pronounced in the intermediate-coupling and strong-coupling regimes. However, by adjusting the on-site interaction parameter, it was possible to recover the correction in the electric energy term (50) substantially, and hence the ionic Hubbard dynamics is now closer to the

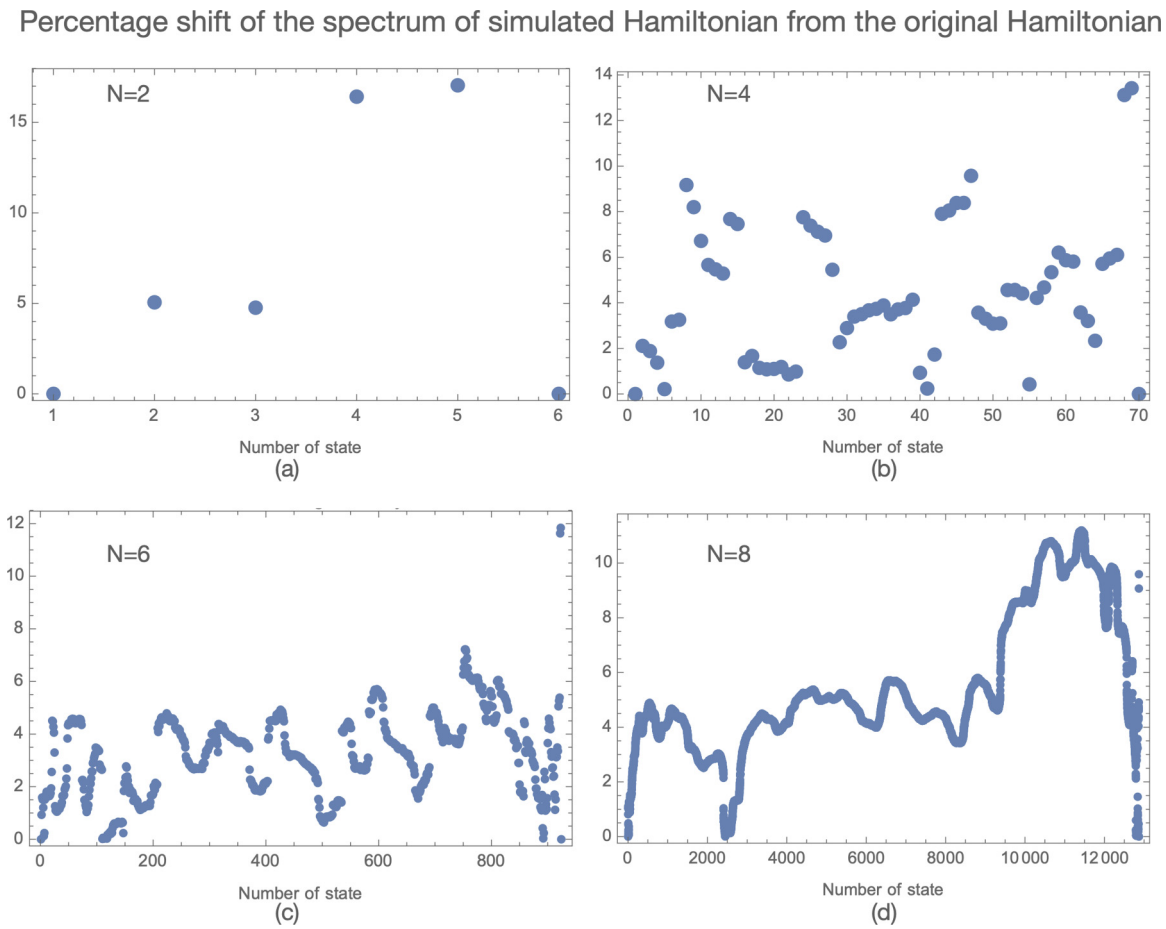

FIG. 4. Spectrum of the simulated Hamiltonian compared with the spectrum of the full gauge theory Hamiltonian. In this comparative study, the incoming flux for the lattice of size N is taken to be $l_i = N$, and the experimental parameters are adjusted accordingly to simulate the gauge theory with the coupling $x_0 = 1$. The deviation of the simulated eigenvalues ranges from (a) 0–17% for $N = 2$ to (b) 0–14% for $N = 4$ to (c, d) 0–12% for $N = 6$ and 8. This shows that the simulated dynamics becomes more reliable as the lattice size increases. As explained in the text, in the bulk limit of the lattice, the simulated Hamiltonian would match the original gauge theory Hamiltonian as the natural consequence of statistical distribution of the fermions on the lattice. However, classical simulation is not the perfect tool to predict that statistical result (with at least N 100+) via exact diagonalization of the Hamiltonian as the dimension of the Hilbert space is 2^{2N}.

dynamics of the full gauge theory, when compared to the same with the approximated LSH formulation.

(3) The discrepancy that still exists in the intermediate- and strong-coupling regimes will surely get reduced if one can simulate using a long enough lattice, such that in the statistical limit, one can really recover the correction in electric energy term (50) in full by choosing the atomic self-interaction accordingly. Considering that we used a small lattice (six site system) for our numerical simulation and yet managed to observe a good agreement, it is extremely likely that in an actual experiment (or tensor network calculation) involving a large number of lattice sites, the error will be insignificant.

It is discussed in Sec. IV how one can measure the dynamics in an actual experiment. However, the actual time measured in ms during the experiment is related to the scaled times as

$$\tau_{\text{exp}} = \frac{\hbar \tau_{\text{atomic}}}{t} \equiv \frac{\tau_{\text{atomic}}}{1.5716}\text{ms} \tag{79}$$

$$\Rightarrow \equiv \frac{2a\tau_{\text{gauge}}}{1.5716}\text{ms}. \tag{80}$$

Thus, for different values of lattice spacing, the same experiment would simulate real-time dynamics of gauge theory happening in a different smaller time scale.

C. Effects of possible experimental errors

As discussed in Sec. IV D, the dominant contribution to the experimental error would come from an imperfection in the initial-state preparation. To obtain a rough estimate of the same, we study the simulated dynamics for a six site lattice. Ideally, all the odd sites should be doubly occupied. We choose two other configurations: (i) two odd sites doubly occupied, a singly occupied odd site, and a singly occupied even site (an error of ≈17%) and (ii) two odd sites doubly occupied and a doubly occupied even site (an error of ≈33%). As shown in Fig. 7, the error is large in a very short time span only (<0.5 in units of the scaled time τ, while the dynamics was studied in the range 0 to 10 in the same unit). If we exclude this region, the percentage error in the first case is well within the margin of 10% for most of the course of evolution, and its peak value lies at around 20%. In the second

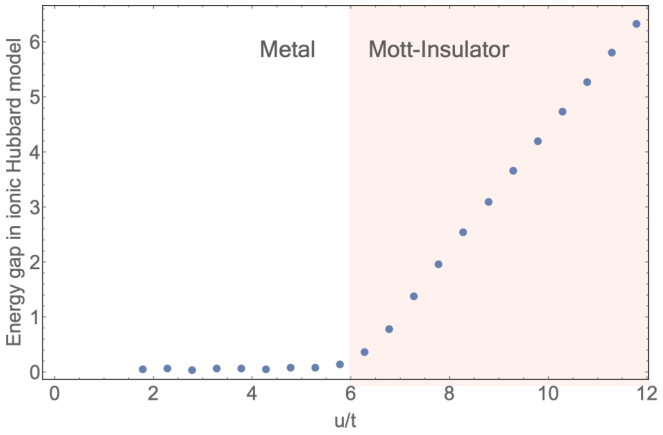

FIG. 5. A quantum phase transition observed with the ionic Hubbard model at a particular value of u/t, beyond which the spectrum becomes gapped and hence the Hubbard model can no longer mimic the dynamics of gauge theory. This particular plot is obtained with the parameters of the Hubbard model given in (77) except varying u/t. Choosing a larger value of V_0/t corresponds to a smaller value of x_0 via (70), but following (71) it will always be in the Mott insulating phase.

case, the percentage error lies well within the margin of 20% for most of the course of evolution, and its peak value lies slightly above 40%. Thus, one may conclude that as long as the error in the initial-state preparation is within a reasonable range (like, in [61], the systematic uncertainty is 10%), the dynamics is not much affected by it.

VI. DISCUSSIONS AND FUTURE DIRECTIONS

This paper presents the very first practically implementable quantum simulation proposal for simulating $SU(2)$ lattice gauge theory in $(1+1)$ dimensions, that specifically simulates the spectrum and dynamics of gauge theory in the weak-coupling regime as well as intermediate-coupling regime for a large lattice with good accuracy. Experimental implementation of this particular scheme will demonstrate why quantum simulators can be a very effective tool to study different aspects of gauge theories.

The experimental scheme is remarkably simple. The parameter regimes that we prescribe are very well accessible in current experiments with ultracold atoms. Moreover, the fact that it is only the averaged population imbalance between the odd and even sites that is to be measured (and not the single site resolved statistics) makes it easier to implement. The only possible source of experimental error could be that in the initial-state preparation where the CDW state might not be a perfect one. We have shown in our simulation that such an error affects the dynamics in a very short initial time window only. The atomic dynamics, as observed in a longer time scale, can very well simulate the gauge theory dynamics: creation of particle-antiparticle pairs and breaking of strings.

The proposal is completely scalable and accesses different regimes of gauge theory (with a varying degree of accuracy) and quantum simulates different symmetry sectors. A suitable scaling scheme presented in this paper enables one to model different regimes of LGT with a single experimental setup, just by tuning the controllable experimental parameters. For example, the weak- and strong-coupling limits of gauge theory are accessed by taking u/t to 0 and $u < u_c$, respectively, in the atomic system, where u_c is a quantum critical point beyond which the atomic system enters into a Mott insulating phase as observed in this particular study with small lattice (see Fig. 5). The only requirement here is that the system is required to remain in the same paramagnetic phase throughout the course of its dynamics, so that in a bulk limit, all the allowed states are equally probable at half filling.

The scheme we present here has a wider applicability compared to its past counterparts, due to the following reasons.

(a) Any formalism that deals with the purely fermionic degrees of freedom of gauge theory (involving a complete gauge fixing) is dimension specific, whereas, in the LSH framework, the treatment remains valid for all dimensions. Here the coupling of matter to the gauge field remains the same as in the 1D lattice for any higher dimension. Hence, construction of any building block, as done in one dimension, will remain useful for higher-dimensional models as well.

(b) Replacing gauge fields by fermions as a solution of Gauss law constraint introduces long-range fermionic interactions in the Hamiltonian. However, in the present paper, with the mean-field approximation of the loop degrees of freedom of the gauge theory, the Hamiltonian contains only on-site interactions for the fermions that characterize the combined boson-fermion (ends of string) excitations. Inclusion of the dynamical loop degrees of freedom as in (13), along with Abelian Gauss law constraint (A14), gives the complete and most general description of the theory. Then it becomes exactly equivalent to the purely fermionic formulation [6,13] in one spatial dimension [48].

Future works will address the issue of going beyond mean-field approximation, as well as going beyond one spatial dimension. The LSH formalism for gauge theories in higher dimensions should be equally useful in constructing atomic quantum simulators for the same. Specifically, within the LSH framework, the matter gauge coupling remains the same as in one dimension in any higher dimension, including the feature of nondynamic loop degrees of freedom at matter sites [14,56,58]. Hence we expect the present proposal to remain as a useful building block for higher-dimensional quantum simulators as well. Work is in progress in these directions and will be reported elsewhere. The present scheme can also be generalized for gauge group $SU(3)$ upon generalization of the LSH formalism for $SU(3)$ gauge theory and that will build a concrete step towards quantum simulating QCD.

ACKNOWLEDGMENTS

We would like to thank Z. Davoudi and R. Basu for useful discussions and also for careful reading of the paper and helpful comments. We thank T. Esslinger for useful comments on the source of experimental errors in the present paper. R.D. would like to acknowledge support from the Department of Science and Technology, Government of India in the form of an Inspire Faculty Award (Grant No. 04/2014/002342). I.R. is supported by the U.S. Department of Energy, Office of Science, Office of Advanced Scientific Computing

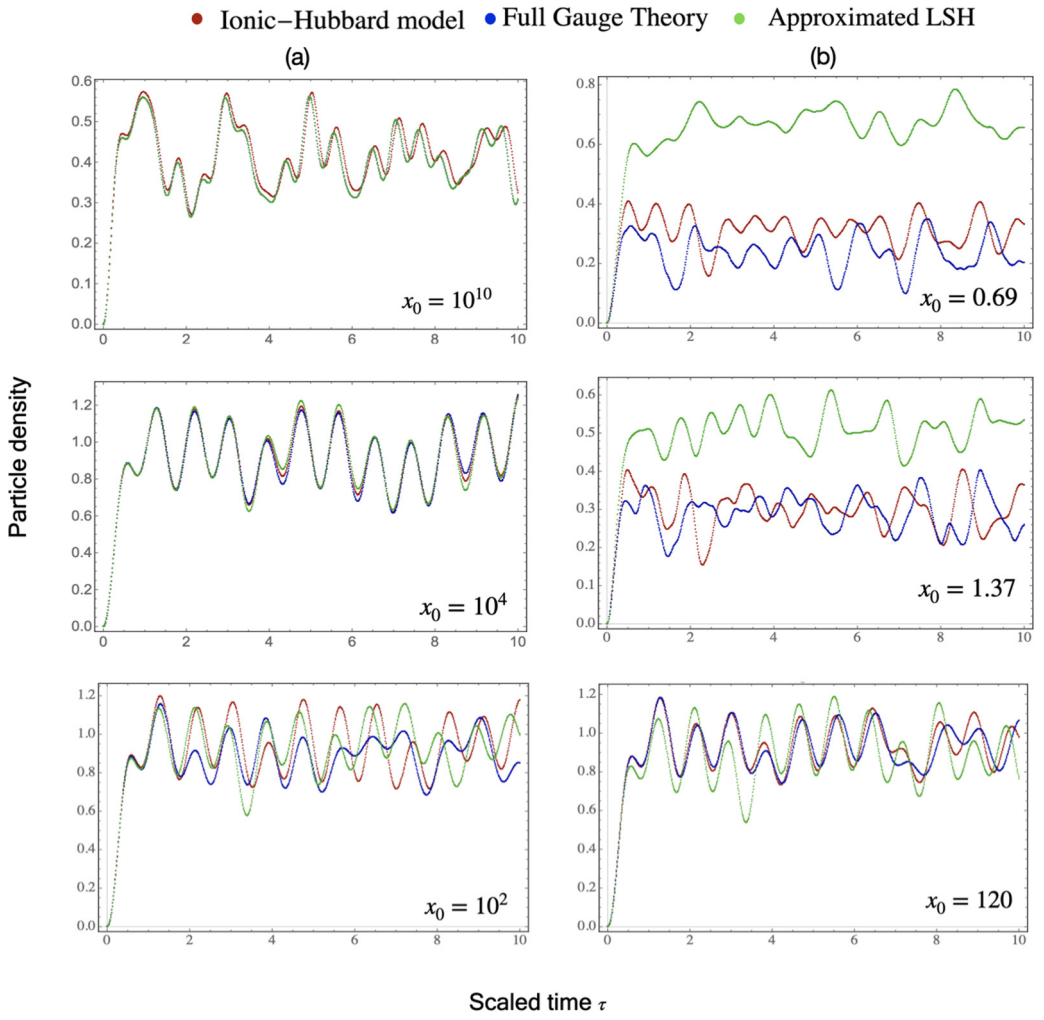

FIG. 6. Simulated particle density dynamics, corresponding to Fig. 2(a), plotted against a scaled time τ. The parameters are identical to that used for spectrum analysis in Fig. 3 for the (a) weak-coupling regime and (b) strong-coupling regime. The simulated dynamics is almost exactly identical to that of the full gauge theory for the weak-coupling limit. The mismatch between full gauge theory dynamics and Hubbard model dynamics in the strong-coupling regime is expected to get minimized at the bulk limit. The approximated LSH is only valid in the weak-coupling regime and matches with full gauge theory for $p \gg 1$ as demonstrated in spectrum analysis as well. The simulated dynamics is matching better with the full gauge theory dynamics than that of the approximated Hamiltonian. This is because the tuned self-interaction of the atomic Hamiltonian takes care of a significant error that exists in the approximated Hamiltonian.

Research Quantum Computing Application Teams program, under fieldwork Proposal No. ERKJ347.

APPENDIX A: LOOP-STRING-HADRON HAMILTONIAN

LSH formalism of lattice gauge theory is based on the prepotential framework, where the original canonical conjugate variables of the theory, i.e., color electric field and link operators, are replaced by a set of harmonic oscillator doublets, defined at each end of a link [58,74–81]. In the prepotential framework, the $SU(2)$ gauge group is confined to each lattice site allowing one to have local gauge invariant operators and states at each site. For pure gauge theory, these local gauge invariant operators and states can be interpreted as local snapshots of Wilson loop operators of original gauge theory. One can now construct local loop Hilbert space by action of local loop operators on strong-coupling vacuum of the theory (no flux state) defined locally at each site. At this point, we must mention that mapping the local loop picture to the original loop description of gauge theory requires one extra constraint on each link, that states

$$N_L(j) = N_R(j) \tag{A1}$$

where $N_{L(R)}$ is the occupation number of prepotentials or Schwinger bosons at the left (right) end of a link connecting sites j and $j+1$. This constraint is actually a consequence of the constraint $\boldsymbol{E}_L^2 = \boldsymbol{E}_R^2$ mentioned in Sec. II.

Inclusion of staggered fermionic matter fields for $SU(2)$ gauge theory at each lattice site combines smoothly with the local loop description obtained in the prepotential framework as both the prepotential Schwinger bosons and matter fields transform as fundamental representations of the local $SU(2)$ at that site. In addition to local gauge invariant loop operators, one can now combine matter and prepotentials to construct local string operators, that denote the start of a string from a particle and/or end of a string at an antiparticle. Matter fields

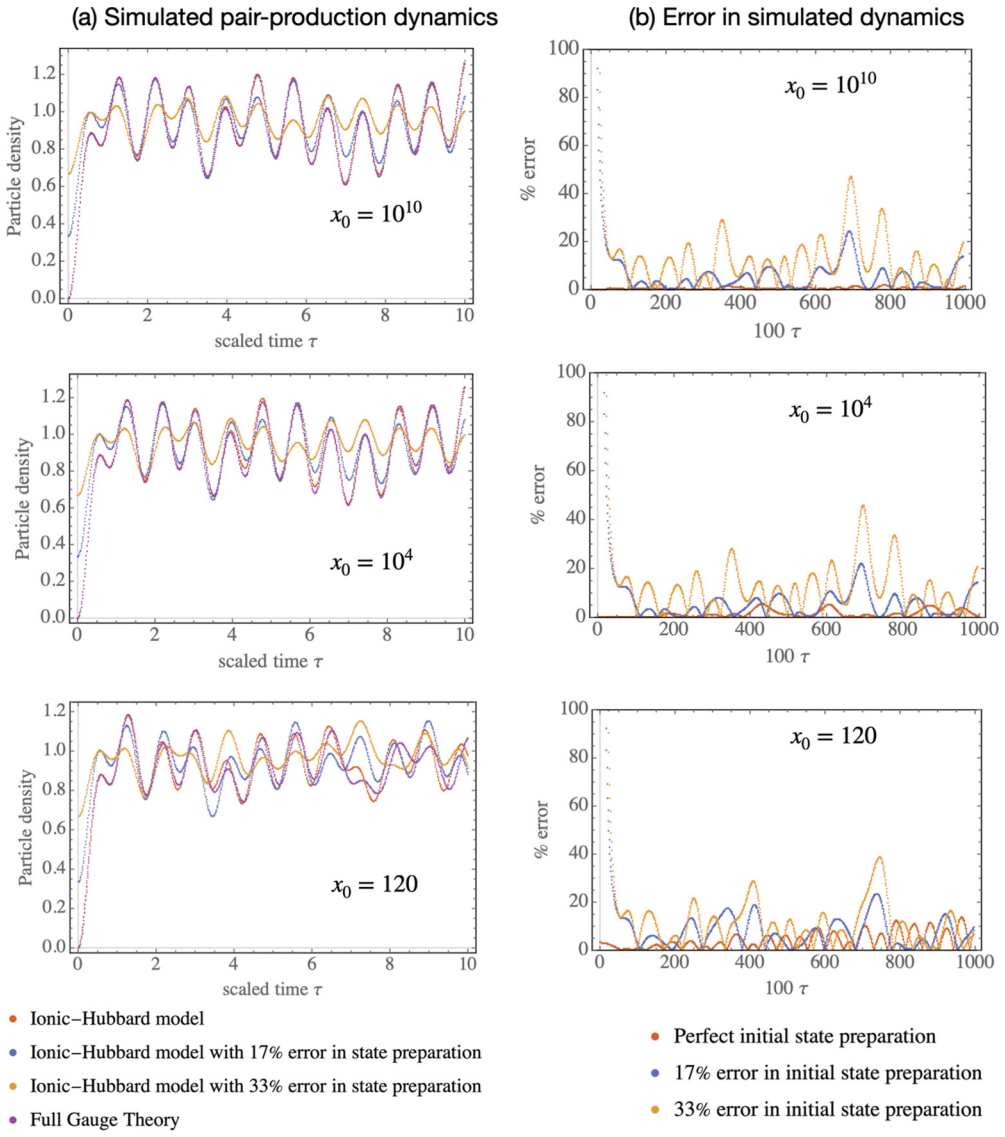

FIG. 7. (a) The particle number dynamics of the original theory compared against the simulated dynamics for different values of the coupling x_0. (b) Percentage deviation from the dynamics of the original theory for the perfectly prepared initial state as well as imperfect initial-state preparation compared. A lattice of six sites is being considered. The initial state of the system is chosen to be the strong-coupling vacuum, where the alternate sites (odd sites) are fully filled by fermions and other sites (even sites are empty). We consider imperfect initial states with (i) one fermion at one of its even sites and one odd site half filled that corresponds to almost 17% error in the initial-state preparation and (ii) one fully filled even site and one fully vacant odd site, representing almost 33% error in the initial-state preparation.

combine into local gauge invariant configurations representing hadrons likewise in the original formalism. This complete description is named as the LSH formalism as in [14]. We are not going into the details of the full LSH formalism here. Instead, we will focus on the application of LSH formulation to one spatial dimension only, and describe the appropriate framework.

Within the LSH framework, the gauge invariant and orthonormal LSH basis is characterized by a set of three integers $n_l(j), n_i(j),$ and $n_o(j)$ that satisfies Gauss's law constraint:

$$G^a(j)|n_l(j), n_i(j), n_o(j)\rangle = 0, \quad \forall j, a. \tag{A2}$$

These three quantum numbers signify the loop, incoming string, and outgoing string at each site. The allowed values of these integers are given by

$$0 \leqslant n_l(j) \leqslant \infty, \tag{A3}$$

$$0 \leqslant n_i(j) \leqslant 1, \tag{A4}$$

$$0 \leqslant n_O(j) \leqslant 1. \tag{A5}$$

Pictorially, the LSH quantum numbers are illustrated in Fig. 8. It is clear from the range of the quantum numbers that n_l is bosonic excitation, whereas n_i and n_o are fermionic in nature. However, it is important to note that, unlike the fermionic matter field in the original theory, the fermionic operators building the "local string" Hilbert space are $SU(2)$ invariant bilinears of one bosonic prepotential operator and one fermionic matter

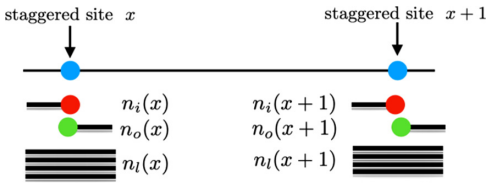

FIG. 8. Two staggered sites in the LSH formulation on a 1D spatial lattice. Each site carries three types of operators, namely, incoming string, outgoing string, and flux. The Hilbert space is characterized by the corresponding quantum numbers n_l, n_i, and n_o, respectively, for each and every site of the lattice.

field, yielding overall fermionic statistics. Hence, the string states contain the information of both gauge field and matter content.

At this point, we define a set of LSH operators consisting of both diagonal and ladder operators locally at each site as follows:

$$\hat{n}_l|n_l, n_i, n_o\rangle = n_l|n_l, n_i, n_o\rangle, \tag{A6}$$

$$\hat{n}_i|n_l, n_i, n_o\rangle = n_i|n_l, n_i, n_o\rangle, \tag{A7}$$

$$\hat{n}_o|n_l, n_i, n_o\rangle = n_o|n_l, n_i, n_o\rangle, \tag{A8}$$

$$\hat{\lambda}^{\pm}|n_l, n_i, n_o\rangle = |n_l \pm 1, n_i, n_o\rangle, \tag{A9}$$

$$\hat{\chi}_i^{+}|n_l, n_i, n_o\rangle = (1-\delta_{n_i,1})|n_l, n_i+1, n_o\rangle, \tag{A10}$$

$$\hat{\chi}_i^{-}|n_l, n_i, n_o\rangle = (1-\delta_{n_i,0})|n_l, n_i-1, n_o\rangle, \tag{A11}$$

$$\hat{\chi}_o^{+}|n_l, n_i, n_o\rangle = (1-\delta_{n_o,1})|n_l, n_i, n_o+1\rangle, \tag{A12}$$

$$\hat{\chi}_o^{-}|n_l, n_i, n_o\rangle = (1-\delta_{n_o,0})|n_l, n_i, n_o-1\rangle. \tag{A13}$$

In the above set of equations, we have not mentioned the explicit site index as these are considered to be defined at a particular site.

One major benefit of using the LSH formalism is that one no longer needs to solve or satisfy the $SU(2)$ Gauss law (7) at each site as the basis states are $SU(2)$ gauge invariant by construction. Note that, for non-Abelian gauge theories, imposing Gauss's law is a nontrivial task and that gives rise to a whole range of complications as discussed in [48]. However, the LSH formalism still carries the constraint (A1) that is necessary to glue $SU(2)$ invariant states residing at neighboring sites to yield original nonlocal gauge invariant Hilbert space of the theory. In terms of LSH operators, this constraint (A1) reads as

$$\begin{aligned}&\hat{n}_l(j) + \hat{n}_o(j)[1-\hat{n}_i(j)]\\ &= \hat{n}_l(j+1) + \hat{n}_i(j+1)[1-\hat{n}_o(j+1)].\end{aligned} \tag{A14}$$

Comparing each side of (A14) to that of (A1) upon acting on LSH basis states, we get

$$N_L(j) = n_l(j) + n_o(j)[1-n_i(j)], \tag{A15}$$

$$N_R(j) = n_l(j+1) + n_i(j+1)[1-n_o(j+1)] \tag{A16}$$

where $N_L(j)$ and $N_R(j)$ count bosonic occupation numbers at each end of the link connecting site j and $j+1$. As mentioned earlier, the bosonic occupation number at each end of a link has contribution coming from fermionic excitation n_i and n_o as well. Pictorially, the left and right side of (A14) and/or (A1) is represented by the number of thick solid lines at the left and right end of a link connecting sites j and $j+1$ in Fig. 8. As in [14,48], the definition of a hadronic state in the LSH basis is given by $|n_l = 0, n_i = 1, n_o = 1\rangle$ at one particular site.

The Hamiltonian of the theory, exactly equivalent to the original Hamiltonian (1) in terms of LSH operators, is given by

$$H^{(\mathrm{LSH})} = H_E^{(\mathrm{LSH})} + H_M^{(\mathrm{LSH})} + H_I^{(\mathrm{LSH})} \tag{A17}$$

where $H_E^{(\mathrm{LSH})}$ is the electric energy term, $H_M^{(\mathrm{LSH})}$ is the mass term, and $H_I^{(\mathrm{LSH})}$ is the matter-gauge interaction term of the Hamiltonian. Explicitly, in terms of LSH operators defined in (A6)–(A13), each part of the Hamiltonian is as below:

$$\begin{aligned}H_E^{(\mathrm{LSH})} = \frac{g^2 a}{2}\sum_n \Bigg[&\frac{\hat{n}_l(j) + \hat{n}_o(j)[1-\hat{n}_i(j)]}{2}\\ &\times\left(\frac{\hat{n}_l(j) + \hat{n}_o(j)[1-\hat{n}_i(j)]}{2} + 1\right)\Bigg]\end{aligned} \tag{A18}$$

$$H_M^{(\mathrm{LSH})} = m\sum_n (-1)^j[\hat{n}_i(j) + \hat{n}_o(j)], \tag{A19}$$

$$\begin{aligned}H_I^{(\mathrm{LSH})} = \frac{1}{2a}\sum_n &\frac{1}{\sqrt{\hat{n}_l(j) + \hat{n}_o(j)[1-\hat{n}_i(j)]+1}}\\ &\times[S_o^{++}(j)S_i^{+-}(j+1) + S_o^{--}(j)S_i^{-+}(j+1)\\ &+S_o^{+-}(j)S_i^{--}(j+1) + S_o^{-+}(j)S_i^{++}(j+1)]\\ &\times\frac{1}{\sqrt{\hat{n}_l(j+1) + \hat{n}_i(j+1)[1-\hat{n}_o(j+1)]+1}}.\end{aligned} \tag{A20}$$

Here (A20) contains LSH ladder operators in the following combinations (suppressing the explicit site index):

$$S_o^{++} = \hat{\chi}_o^{+}(\lambda^{+})^{\hat{n}_i}\sqrt{\hat{n}_l + 2 - \hat{n}_i}, \tag{A21}$$

$$S_o^{--} = \hat{\chi}_o^{-}(\lambda^{-})^{\hat{n}_i}\sqrt{\hat{n}_l + 2(1-\hat{n}_i)}, \tag{A22}$$

$$S_o^{+-} = \hat{\chi}_i^{+}(\lambda^{-})^{1-\hat{n}_o}\sqrt{\hat{n}_l + 2\hat{n}_o}, \tag{A23}$$

$$S_o^{-+} = \hat{\chi}_i^{-}(\lambda^{+})^{1-\hat{n}_o}\sqrt{\hat{n}_l + 1 + \hat{n}_o)} \tag{A24}$$

and

$$S_i^{+-} = \hat{\chi}_o^{-}(\lambda^{+})^{1-\hat{n}_i}\sqrt{\hat{n}_l + 1 + \hat{n}_i)}, \tag{A25}$$

$$S_i^{-+} = \hat{\chi}_o^{+}(\lambda^{-})^{1-\hat{n}_i}\sqrt{\hat{n}_l + 2\hat{n}_i}, \tag{A26}$$

$$S_i^{--} = \hat{\chi}_i^{-}(\lambda^{-})^{\hat{n}_o}\sqrt{\hat{n}_l + 2(1-\hat{n}_o)}, \tag{A27}$$

$$S_i^{++} = \hat{\chi}_i^{+}(\lambda^{+})^{\hat{n}_o}\sqrt{\hat{n}_l + 2 - \hat{n}_o}. \tag{A28}$$

The strong-coupling ($ga \gg 1$, ma =fixed) vacuum of the LSH Hamiltonian is given by

$$\begin{aligned} &n_l(j) = 0\ \forall j, \\ &n_i(j) = 1, n_o(j) = 1 \text{ for } j \text{ odd}, \\ &n_i(j) = 0, n_o(j) = 0 \text{ for } j \text{ even}. \end{aligned} \tag{A29}$$

It is easy to check that (A29) satisfies Abelian Gauss law (A14). One should also consider a suitable boundary condition for the one-dimensional spatial lattice as discussed in detail in [48] as

open boundary condition (OBC),

$$N_R(0) = l_i^{\text{OBC}};$$

periodic boundary condition (PBC),

$$N_R(0) = N_L(N-1) \equiv l_i^{\text{PBC}}$$

where N_L, N_R are defined in (A15) and (A16) for the first (0) and last $(N-1)$ site of a N site lattice. l_i can be any positive semidefinite integer. Now, one can easily check that, for any gauge invariant state $\prod_{j=0}^{N-1} |n_l(j), n_i(j), n_o(j)\rangle$, the bosonic quantum numbers $n_l(j)$ for all values of j are completely determined by the boundary flux l_i and constraint (A14) imposed on each and every link of the lattice starting from one end as

$$n_l(j) = l_i + \sum_{y=0}^{j-1} [n_o(y) - n_i(y)] - n_i(j)[1 - n_o(j)]. \tag{A30}$$

For OBC, any physical state in the LSH formalism is completely determined by (n_i, n_o) quantum numbers at each side. For PBC, the gauge invariant or LSH Hilbert space is characterized by many copies of the same fermionic (n_i, n_o) configurations with different winding number of closed loops, that plays the exact role as the l_i and fixes the n_l's throughout the lattice. We exploit this particular feature in the analog quantum simulation proposal outlined in the present paper.[3] Note that n_l being determined does not mean that we describe a static gauge field theory; rather, truly relevant or physical gauge degrees of freedom are contained in the (n_i, n_o) excitation of any physical state.

APPENDIX B: FERMI-HUBBARD MODEL AND TIGHT-BINDING PARAMETERS

Let $\psi_\uparrow(x)$ and $\psi_\downarrow(x)$ be the field operators corresponding to the two hyperfine states of the fermionic atom. Now, if the lattice potentials are sufficiently deep, the field operators can be expanded in terms of single-particle Wannier functions, localized to each lattice site:

$$\psi_\sigma(x) = \sum_j c_\sigma(j)\mathcal{W}(x - x_j), \qquad \sigma = \uparrow, \downarrow, \tag{B1}$$

where $c_\sigma(j)$ is the fermionic annihilation operator for spin index σ and site j. The corresponding number operators are $\mathcal{N}_{j\sigma} = c_\sigma^\dagger(j)c_\sigma(j)$.

[3]The numerical analysis performed in this paper is for OBC in gauge theory as simulating the same in an experiment is easier than that for PBC.

The Hamiltonian can be written as

$$H = H_{\text{hopping}} + H_{\text{int}} + H_0. \tag{B2}$$

Here H_{hopping} denotes the hopping of a fermion from one site to another, H_{int} represents the interaction when one up-spin fermion shares the same site with a down-spin fermion, and H_0 is the energy offset, arising out of the single-particle Hamiltonian.

Let

$$\mathcal{H}_0(x) = \frac{-\hbar^2}{2m}\frac{\partial^2}{\partial x^2} + V(x). \tag{B3}$$

In our construction, $V(x) = -V_L \cos x^2$. So, effectively, $V(x) = -V_L$ for each site.

1. Hopping

The hopping term, which represents the tunneling between sites, is given by

$$H_{\text{hopping}} = -\sum_{ij} t_{i,j}[c_\uparrow^\dagger(j)c_\uparrow(i) + c_\downarrow^\dagger(j)c_\downarrow(i)]. \tag{B4}$$

Tunneling to next-nearest neighbors is usually suppressed by one order of magnitude, in comparison with the nearest-neighbor tunneling. So we consider hopping between adjacent sites only. The tunneling rate from site j to $(j+1)$ is given by the matrix element

$$t_{j,(j+1)} = -\int \mathcal{W}(x - x_j)\mathcal{H}_0\mathcal{W}(x - x_{j+1})dx. \tag{B5}$$

2. On-site interaction term

In the low-energy scattering regime, the atoms usually interact via s-wave scattering. The corresponding coupling constant is given by

$$g_0 = \frac{4\pi\hbar^2 a_s}{m},$$

a_s being the scattering length. The interacting part of the Hamiltonian (between up-spin and down-spin fermions sharing the same site) is given by

$$H_{\text{int}} = u\sum_j \mathcal{N}_\uparrow(j)\mathcal{N}_\downarrow(j). \tag{B6}$$

Here the on-site interaction matrix element is given by

$$u = g_0 \int |\mathcal{W}(x - x_j)|^4 dx. \tag{B7}$$

3. Energy offset

The energy offset can be expressed as

$$H_0 = \sum_j \epsilon_j \mathcal{N}(j), \tag{B8}$$

where

$$\epsilon_j = \int \mathcal{W}(x - x_j)\mathcal{H}_0\mathcal{W}(x - x_j)dx. \tag{B9}$$

In our construction, the lattice potential $V(x) = -V_L \cos kx^2$, and in Sec. III A we split this potential as

$V_L = V_1 - V_0$. At this point, we drop the contribution from the kinetic term and also V_1, because these simply add a constant energy shift throughout the lattice. H_{V_0}, the contribution from V_0, is a constant, too, but we keep this, in order to make a direct correspondence with the reduced LSH Hamiltonian:

$$H_{V_0} = \sum_j V_0 \mathcal{N}(j). \tag{B10}$$

Next, alternating potentials V' and $-V'$ are added to the odd and even sites, respectively. Thus the relevant part of the energy offset becomes

$$H_0 = H_{V_0} + H_{V'} \tag{B11}$$

with

$$H_{V'} = V' \sum_{j=\text{odd}} \mathcal{N}(j) - V' \sum_{j=\text{even}} \mathcal{N}(j). \tag{B12}$$

[1] K. G. Wilson, Confinement of quarks, Phys. Rev. D **10**, 2445 (1974).

[2] M. Creutz, L. Jacobs, and C. Rebbi, Monte Carlo computations in lattice gauge theories, Phys. Rep. **95**, 201 (1983).

[3] B. Joó, C. Jung, N. H. Christ, W. Detmold, R. G. Edwards, M. Savage, and P. Shanahan, Status and future perspectives for lattice gauge theory calculations to the exascale and beyond, Eur. Phys. J. A **55**, 199 (2019).

[4] P. de Forcrand, Simulating QCD at finite density, PoS **LAT2009**, 010 (2009).

[5] R. P. Feynman, Simulating physics with computers, Int. J. Theor. Phys. **21**, 467 (1982).

[6] M. C. Banuls, R. Blatt, J. Catani, A. Celi, J. I. Cirac, M. Dalmonte, L. Fallani, K. Jansen, M. Lewenstein, S. Montangero *et al.*, Simulating lattice gauge theories within quantum technologies, Eur. Phys. J. D **74**, 165 (2020).

[7] Z. Davoudi, M. Hafezi, C. Monroe, G. Pagano, A. Seif, and A. Shaw, Towards analog quantum simulations of lattice gauge theories with trapped ions, Phys. Rev. Research **2**, 023015 (2020).

[8] N. Klco, E. F. Dumitrescu, A. J. McCaskey, T. D. Morris, R. C. Pooser, M. Sanz, E. Solano, P. Lougovski, and M. J. Savage, Quantum-classical computation of schwinger model dynamics using quantum computers, Phys. Rev. A **98**, 032331 (2018).

[9] N. Klco, M. J. Savage, and J. R. Stryker, Su (2) non-Abelian gauge field theory in one dimension on digital quantum computers, Phys. Rev. D **101**, 074512 (2020).

[10] A. F. Shaw, P. Lougovski, J. R. Stryker, and N. Wiebe, Quantum algorithms for simulating the lattice schwinger model, Quantum **4**, 306 (2020).

[11] Z. Davoudi, N. M. Linke, and G. Pagano, Toward simulating quantum field theories with controlled phonon-ion dynamics: A hybrid analog-digital approach, Phys. Rev. Research **3**, 043072 (2021).

[12] A. Ciavarella, N. Klco, and M. J. Savage, Trailhead for quantum simulation of su (3) yang-mills lattice gauge theory in the local multiplet basis, Phys. Rev. D **103**, 094501 (2021).

[13] Y. Atas, J. Zhang, R. Lewis, A. Jahanpour, J. F. Haase, and C. A. Muschik, SU(2) hadrons on a quantum computer via a variational approach, Nat. Commun. **12**, 6499 (2021).

[14] I. Raychowdhury and J. R. Stryker, Loop, string, and hadron dynamics in $SU(2)$ hamiltonian lattice gauge theories, Phys. Rev. D **101**, 114502 (2020).

[15] I. Bloch, J. Dalibard, and S. Nascimbene, Quantum simulations with ultracold quantum gases, Nat. Phys. **8**, 267 (2012).

[16] R. Blatt and C. F. Roos, Quantum simulations with trapped ions, Nat. Phys. **8**, 277 (2012).

[17] M. H. Anderson, J. R. Ensher, M. R. Matthews, C. E. Wieman, and E. A. Cornell, Observation of Bose-Einstein condensation in a dilute atomic vapor, Science **269**, 198 (1995).

[18] C. C. Bradley, C. A. Sackett, J. J. Tollett, and R. G. Hulet, Evidence of Bose-Einstein Condensation in an Atomic Gas with Attractive Interactions, Phys. Rev. Lett. **75**, 1687 (1995).

[19] K. B. Davis, M.-O. Mewes, M. R. Andrews, N. J. van Druten, D. S. Durfee, D. M. Kurn, and W. Ketterle, Bose-Einstein Condensation in a Gas of Sodium Atoms, Phys. Rev. Lett. **75**, 3969 (1995).

[20] B. DeMarco and D. S. Jin, Onset of fermi degeneracy in a trapped atomic gas, Science **285**, 1703 (1999).

[21] F. Schreck, L. Khaykovich, K. L. Corwin, G. Ferrari, T. Bourdel, J. Cubizolles, and C. Salomon, Quasipure Bose-Einstein Condensate Immersed in a Fermi Sea, Phys. Rev. Lett. **87**, 080403 (2001).

[22] A. G. Truscott, K. E. Strecker, W. I. McAlexander, G. B. Partridge, and R. G. Hulet, Observation of fermi pressure in a gas of trapped atoms, Science **291**, 2570 (2001).

[23] K. O'hara, S. Hemmer, M. Gehm, S. Granade, and J. Thomas, Observation of a strongly interacting degenerate fermi gas of atoms, Science **298**, 2179 (2002).

[24] M. Greiner, C. A. Regal, and D. S. Jin, Emergence of a molecular Bose-Einstein condensate from a Fermi gas, Nature (London) **426**, 537 (2003).

[25] S. Jochim, M. Bartenstein, A. Altmeyer, G. Hendl, S. Riedl, C. Chin, J. H. Denschlag, and R. Grimm, Bose-einstein condensation of molecules, Science **302**, 2101 (2003).

[26] M. W. Zwierlein, Z. Hadzibabic, S. Gupta, and W. Ketterle, Spectroscopic Insensitivity to Cold Collisions in a Two-State Mixture of Fermions, Phys. Rev. Lett. **91**, 250404 (2003).

[27] M. Greiner, O. Mandel, T. Esslinger, T. W. Hänsch, and I. Bloch, Quantum phase transition from a superfluid to a mott insulator in a gas of ultracold atoms, Nature (London) **415**, 39 (2002).

[28] M. Lewenstein, A. Sanpera, V. Ahufinger, B. Damski, A. Sen, and U. Sen, Ultracold atomic gases in optical lattices: mimicking condensed matter physics and beyond, Adv. Phys. **56**, 243 (2007).

[29] M. Lewenstein, A. Sanpera, and V. Ahufinger, *Ultracold Atoms in Optical Lattices: Simulating Quantum Many-Body Systems* (Oxford University, New York, 2012).

[30] C. Gross and I. Bloch, Quantum simulations with ultracold atoms in optical lattices, Science **357**, 995 (2017).

[31] E. Zohar and B. Reznik, Confinement and Lattice Quantum-Electrodynamic Electric Flux Tubes Simulated with Ultracold Atoms, Phys. Rev. Lett. **107**, 275301 (2011).

[32] E. Zohar, J. I. Cirac, and B. Reznik, Cold-Atom Quantum Simulator for $SU(2)$ Yang-Mills Lattice Gauge Theory, Phys. Rev. Lett. **110**, 125304 (2013).

[33] E. Zohar, J. I. Cirac, and B. Reznik, Quantum simulations of gauge theories with ultracold atoms: local gauge invariance from angular momentum conservation, Phys. Rev. A **88**, 023617 (2013).

[34] E. Zohar, J. I. Cirac, and B. Reznik, Quantum simulations of lattice gauge theories using ultracold atoms in optical lattices, Rep. Prog. Phys. **79**, 014401 (2015).

[35] D. Banerjee, M. Dalmonte, M. Muller, E. Rico, P. Stebler, U.-J. Wiese, and P. Zoller, Atomic Quantum Simulation of Dynamical Gauge Fields coupled to Fermionic Matter: From String Breaking to Evolution after a Quench, Phys. Rev. Lett. **109**, 175302 (2012).

[36] D. Banerjee, M. Bögli, M. Dalmonte, E. Rico, P. Stebler, U.-J. Wiese, and P. Zoller, Atomic Quantum Simulation of U(N) and SU(N) Non-Abelian Lattice Gauge Theories, Phys. Rev. Lett. **110**, 125303 (2013).

[37] K. Stannigel, P. Hauke, D. Marcos, M. Hafezi, S. Diehl, M. Dalmonte, and P. Zoller, Constrained Dynamics Via the Zeno Effect in Quantum Simulation: Implementing Non-Abelian Lattice Gauge Theories with Cold Atoms, Phys. Rev. Lett. **112**, 120406 (2014).

[38] D. González-Cuadra, E. Zohar, and J. I. Cirac, Quantum simulation of the Abelian-Higgs lattice gauge theory with ultracold atoms, New J. Phys. **19**, 063038 (2017).

[39] Y. Kuno, S. Sakane, K. Kasamatsu, I. Ichinose, and T. Matsui, Quantum simulation of $(1+1)$-dimensional u(1) gauge-higgs model on a lattice by cold bose gases, Phys. Rev. D **95**, 094507 (2017).

[40] Y. Kuno, K. Kasamatsu, Y. Takahashi, I. Ichinose, and T. Matsui, Real-time dynamics and proposal for feasible experiments of lattice gauge–higgs model simulated by cold atoms, New J. Phys. **17**, 063005 (2015).

[41] L. Tagliacozzo, A. Celi, P. Orland, M. Mitchell, and M. Lewenstein, Simulation of non-abelian gauge theories with optical lattices, Nat. Commun. **4**, 2615 (2013).

[42] E. A. Martinez, C. A. Muschik, P. Schindler, D. Nigg, A. Erhard, M. Heyl, P. Hauke, M. Dalmonte, T. Monz, P. Zoller *et al.*, Real-time dynamics of lattice gauge theories with a few-qubit quantum computer, Nature (London) **534**, 516 (2016).

[43] F. Görg, K. Sandholzer, J. Minguzzi, R. Desbuquois, M. Messer, and T. Esslinger, Realization of density-dependent Peierls phases to engineer quantized gauge fields coupled to ultracold matter, Nat. Phys. **15**, 1161 (2019).

[44] C. Schweizer, F. Grusdt, M. Berngruber, L. Barbiero, E. Demler, N. Goldman, I. Bloch, and M. Aidelsburger, Floquet approach to z2 lattice gauge theories with ultracold atoms in optical lattices, Nat. Phys. **15**, 1168 (2019).

[45] A. Mil, T. V. Zache, A. Hegde, A. Xia, R. P. Bhatt, M. K. Oberthaler, P. Hauke, J. Berges, and F. Jendrzejewski, A scalable realization of local u (1) gauge invariance in cold atomic mixtures, Science **367**, 1128 (2020).

[46] B. Yang, H. Sun, R. Ott, H.-Y. Wang, T. V. Zache, J. C. Halimeh, Z.-S. Yuan, P. Hauke, and J.-W. Pan, Observation of gauge invariance in a 71-site Bose–Hubbard quantum simulator, Nature (London) **587**, 392 (2020).

[47] J. B. Kogut and L. Susskind, Hamiltonian formulation of wilson's lattice gauge theories, Phys. Rev. D **11**, 395 (1975).

[48] Z. Davoudi, I. Raychowdhury, and A. Shaw, Search for efficient formulations for hamiltonian simulation of non-abelian lattice gauge theories, Phys. Rev. D **104**, 074505 (2021).

[49] S. Chandrasekharan and U.-J. Wiese, Quantum link models: A discrete approach to gauge theories, Nucl. Phys. B **492**, 455 (1997).

[50] R. Brower, S. Chandrasekharan, and U.-J. Wiese, QCD as a quantum link model, Phys. Rev. D **60**, 094502 (1999).

[51] E. Zohar and J. I. Cirac, Removing staggered fermionic matter in $U(N)$ and $SU(N)$ lattice gauge theories, Phys. Rev. D **99**, 114511 (2019).

[52] E. Zohar and J. I. Cirac, Eliminating fermionic matter fields in lattice gauge theories, Phys. Rev. B **98**, 075119 (2018).

[53] E. Zohar and M. Burrello, Formulation of lattice gauge theories for quantum simulations, Phys. Rev. D **91**, 054506 (2015).

[54] M. C. Bañuls, K. Cichy, J. I. Cirac, K. Jansen, and S. Kühn, Efficient Basis Formulation for (1+ 1)-Dimensional su (2) Lattice Gauge Theory: Spectral Calculations with Matrix Product States, Phys. Rev. X **7**, 041046 (2017).

[55] P. Sala, T. Shi, S. Kühn, M. C. Banuls, E. Demler, and J. I. Cirac, Variational study of u (1) and su (2) lattice gauge theories with gaussian states in 1+ 1 dimensions, Phys. Rev. D **98**, 034505 (2018).

[56] I. Raychowdhury and J. R. Stryker, Solving Gauss's law on digital quantum computers with loop-string-hadron digitization, Phys. Rev. Research **2**, 033039 (2020).

[57] C. Hamer, SU(2) Yang-Mills theory in (1+1) dimensions: A finite-lattice approach, Nucl. Phys. B **195**, 503 (1982).

[58] I. Raychowdhury, Low energy spectrum of $SU(2)$ lattice gauge theory: An alternate proposal via loop formulation, Eur. Phys. J. C **79**, 235 (2019).

[59] N. Nagaosa and J.-i. Takimoto, Theory of neutral-ionic transition in organic crystals. I. Monte Carlo simulation of modified Hubbard model, J. Phys. Soc. Jpn. **55**, 2735 (1986).

[60] T. Egami, S. Ishihara, and M. Tachiki, Lattice effect of strong electron correlation: Implication for ferroelectricity and superconductivity, Science **261**, 1307 (1993).

[61] M. Messer, R. Desbuquois, T. Uehlinger, G. Jotzu, S. Huber, D. Greif, and T. Esslinger, Exploring Competing Density Order in the Ionic Hubbard Model with Ultracold Fermions, Phys. Rev. Lett. **115**, 115303 (2015).

[62] M. Fabrizio, A. O. Gogolin, and A. A. Nersesyan, From Band Insulator to Mott Insulator in One Dimension, Phys. Rev. Lett. **83**, 2014 (1999).

[63] A. P. Kampf, M. Sekania, G. I. Japaridze, and P. Brune, Nature of the insulating phases in the half-filled ionic Hubbard model, J. Phys.: Condens. Matter **15**, 5895 (2003).

[64] S. Bag, A. Garg, and H. R. Krishnamurthy, Phase diagram of the half-filled ionic Hubbard model, Phys. Rev. B **91**, 235108 (2015).

[65] A. Samanta and R. Sensarma, Superconductivity from doublon condensation in the ionic Hubbard model, Phys. Rev. B **94**, 224517 (2016).

[66] M. Di Liberto, T. Comparin, T. Kock, M. Ölschläger, A. Hemmerich, and C. M. Smith, Controlling coherence via tuning of the population imbalance in a bipartite optical lattice, Nat. Commun. **5**, 5735 (2014).

[67] S. Scherg, T. Kohlert, J. Herbrych, J. Stolpp, P. Bordia, U. Schneider, F. Heidrich-Meisner, I. Bloch, and M. Aidelsburger, Nonequilibrium Mass Transport in the 1D Fermi-Hubbard Model, Phys. Rev. Lett. **121**, 130402 (2018).

[68] J. P. Ronzheimer, M. Schreiber, S. Braun, S. S. Hodgman, S. Langer, I. P. McCulloch, F. Heidrich-Meisner, I. Bloch, and U. Schneider, Expansion Dynamics of Interacting Bosons in Homogeneous Lattices in One and Two Dimensions, Phys. Rev. Lett. **110**, 205301 (2013).

[69] K. Sponselee, L. Freystatzky, B. Abeln, M. Diem, B. Hundt, A. Kochanke, T. Ponath, B. Santra, L. Mathey, K. Sengstock *et al.*, Dynamics of ultracold quantum gases in the dissipative Fermi-Hubbard model, Quantum Sci. Technol. **4**, 014002 (2018).

[70] I. Bloch, J. Dalibard, and W. Zwerger, Many-body physics with ultracold gases, Rev. Mod. Phys. **80**, 885 (2008).

[71] M. Schreiber, S. S. Hodgman, P. Bordia, H. P. Lüschen, M. H. Fischer, R. Vosk, E. Altman, U. Schneider, and I. Bloch, Observation of many-body localization of interacting fermions in a quasirandom optical lattice, Science **349**, 842 (2015).

[72] M. Aidelsburger, M. Atala, M. Lohse, J. T. Barreiro, B. Paredes, and I. Bloch, Realization of the Hofstadter Hamiltonian with Ultracold Atoms in Optical Lattices, Phys. Rev. Lett. **111**, 185301 (2013).

[73] M. Imada, A. Fujimori, and Y. Tokura, Metal-insulator transitions, Rev. Mod. Phys. **70**, 1039 (1998).

[74] M. Mathur, Harmonic oscillator prepotentials in $SU(2)$ lattice gauge theory, J. Phys. A **38**, 10015 (2005).

[75] M. Mathur, Loop approach to lattice gauge theories, Nucl. Phys. B **779**, 32 (2007).

[76] M. Mathur, I. Raychowdhury, and R. Anishetty, SU(N) Irreducible Schwinger Bosons, J. Math. Phys. **51**, 093504 (2010).

[77] R. Anishetty, M. Mathur, and I. Raychowdhury, Irreducible SU(3) Schhwinger Bosons, J. Math. Phys. **50**, 053503 (2009).

[78] R. Anishetty, M. Mathur, and I. Raychowdhury, Prepotential formulation of SU(3) lattice gauge theory, J. Phys. A **43**, 035403 (2010).

[79] R. Anishetty and I. Raychowdhury, $SU(2)$ lattice gauge theory: Local dynamics on nonintersecting electric flux loops, Phys. Rev. D **90**, 114503 (2014).

[80] I. Raychowdhury, Prepotential formulation of lattice gauge theories, Ph.D. thesis, Calcutta University, 2013.

[81] I. Raychowdhury and R. Anishetty, Prepotential formulation of lattice gauge theory, PoS **LATTICE2014**, 313 (2014).